The SWI/SNF chromatin remodeling assemblies BAF and PBAF differentially regulate cell cycle exit and cellular invasion *in vivo*

Jayson J. Smith[1], Yutong Xiao[1], Nithin Parsan[2], Taylor N. Medwig-Kinney[1], Michael A. Q. Martinez[1], Frances E. Q. Moore[1], Nicholas J. Palmisano[1], Abraham Q. Kohrman[3], Mana Chandhok Delos Reyes[4], Rebecca C. Adikes[1], Simeiyun Liu[1,5], Sydney A. Bracht[1,6], Wan Zhang[1], Kailong Wen[7,8], Paschalis Kratsios[7,8], David Q. Matus[1,9]

[1]Department of Biochemistry and Cell Biology, Stony Brook University, Stony Brook, NY 11794, USA

[2]Massachusetts Institute of Technology, Cambridge, MA 02139, USA

[3]Department of Molecular Biology, Princeton University, Princeton, NJ 08544, USA

[4]10 Grant St., Somerville, MA 02145, USA

[5]Molecular, Cellular and Developmental Biology, University of California Santa Cruz, Santa Cruz, CA 95064, USA

[6]Department of Cell Biology, Johns Hopkins University, Baltimore, MD 21205, USA

[7]The Grossman Institute for Neuroscience, Quantitative Biology, and Human Behavior, University of Chicago, Chicago, IL 60637, USA

[8]Department of Neurobiology, University of Chicago, Chicago, IL 60637, USA

[9]Lead Contact

[*]Correspondence: david.matus@stonybrook.edu

25

26 **SUMMARY STATEMENT**

27 Cellular invasion through the basement membrane by the *C. elegans* anchor cell requires
28 both BAF and PBAF SWI/SNF assemblies to arrest the cell cycle and promote the
29 expression of pro-invasive genes.

30

31 **SUMMARY**

32 Chromatin remodelers such as the SWI/SNF complex coordinate metazoan development
33 through broad regulation of chromatin accessibility and transcription, ensuring normal cell
34 cycle control and cellular differentiation in a lineage-specific and temporally restricted
35 manner. Mutations in genes encoding the structural subunits of chromatin, such as
36 histone subunits, and chromatin regulating factors (CRFs) are associated with a variety
37 of disease mechanisms including cancer metastasis, in which cancer co-opts cellular
38 invasion programs functioning in healthy cells during development. Here we utilize
39 *Caenorhabditis elegans* anchor cell (AC) invasion as an *in vivo* model to identify the suite
40 of chromatin agents and CRFs that promote cellular invasiveness. We demonstrate that
41 the SWI/SNF ATP-dependent chromatin remodeling complex is a critical regulator of AC
42 invasion, with pleiotropic effects on both G_0 cell cycle arrest and activation of invasive
43 machinery. Using targeted protein degradation and enhanced RNA interference (RNAi)
44 vectors, we show that SWI/SNF contributes to AC invasion in a dose-dependent fashion,
45 with lower levels of activity in the AC corresponding to aberrant cell cycle entry and
46 increased loss of invasion. Our data specifically implicate the SWI/SNF BAF assembly in
47 the regulation of the G_0 cell cycle arrest in the AC, whereas the SWI/SNF PBAF assembly

promotes AC invasion via cell cycle-independent mechanisms, including attachment to the basement membrane (BM) and activation of the pro-invasive *fos-1*/FOS gene. Together these findings demonstrate that the SWI/SNF complex is necessary for two essential components of AC invasion: arresting cell cycle progression and remodeling the BM. The work here provides valuable single-cell mechanistic insight into how the SWI/SNF assemblies differentially contribute to cellular invasion and how SWI/SNF subunit-specific disruptions may contribute to tumorigeneses and cancer metastasis.

Keywords: Chromatin regulating factors, chromatin remodeling, SWI/SNF, BAF, PBAF, cell invasion, cell cycle exit, *C. elegans*

INTRODUCTION

Cellular invasion through basement membranes (BMs) is a critical step in metazoan development and is important for human health and fitness. Early in hominid development, trophoblasts must invade into the maternal endometrium for proper blastocyst implantation (1). In the context of immunity, leukocytes become invasive upon injury or infection to travel between the bloodstream and interstitial tissues (2,3). Atypical activation of invasive behavior is associated with a variety of diseases, including rheumatoid arthritis wherein fibroblast-like synoviocytes adopt invasive cellular behavior, leading to the expansion of arthritic damage to previously unaffected joints (4,5). Aberrant activation of cell invasion is also one of the hallmarks of cancer metastasis (6).

A variety of *in vitro* and *in vivo* models have been developed to study the process of cellular invasion at the genetic and cellular levels. *In vitro* invasion assays typically involve 3D hydrogel lattices, such as Matrigel, through which cultured metastatic cancer cells will invade in response to chemo-attractants (7). Recently, microfluidic systems have been integrated with collagen matrices to improve these *in vitro* investigations of cellular invasion (8). While *in vitro* invasion models provide an efficient means to study the mechanical aspects of cellular invasion, they are currently unable to replicate the complex microenvironment in which cells must invade during animal development and disease. A variety of *in vivo* invasion models have been studied, including cancer xenograft models in mouse (9–11) and zebrafish (12,13), each having their respective benefits and drawbacks. Over the past ~15 years, *Caenorhabditis elegans* anchor cell (AC) invasion has emerged as a powerful alternative model due to its visually tractable single-cell nature (**Fig 1 A**) (14).

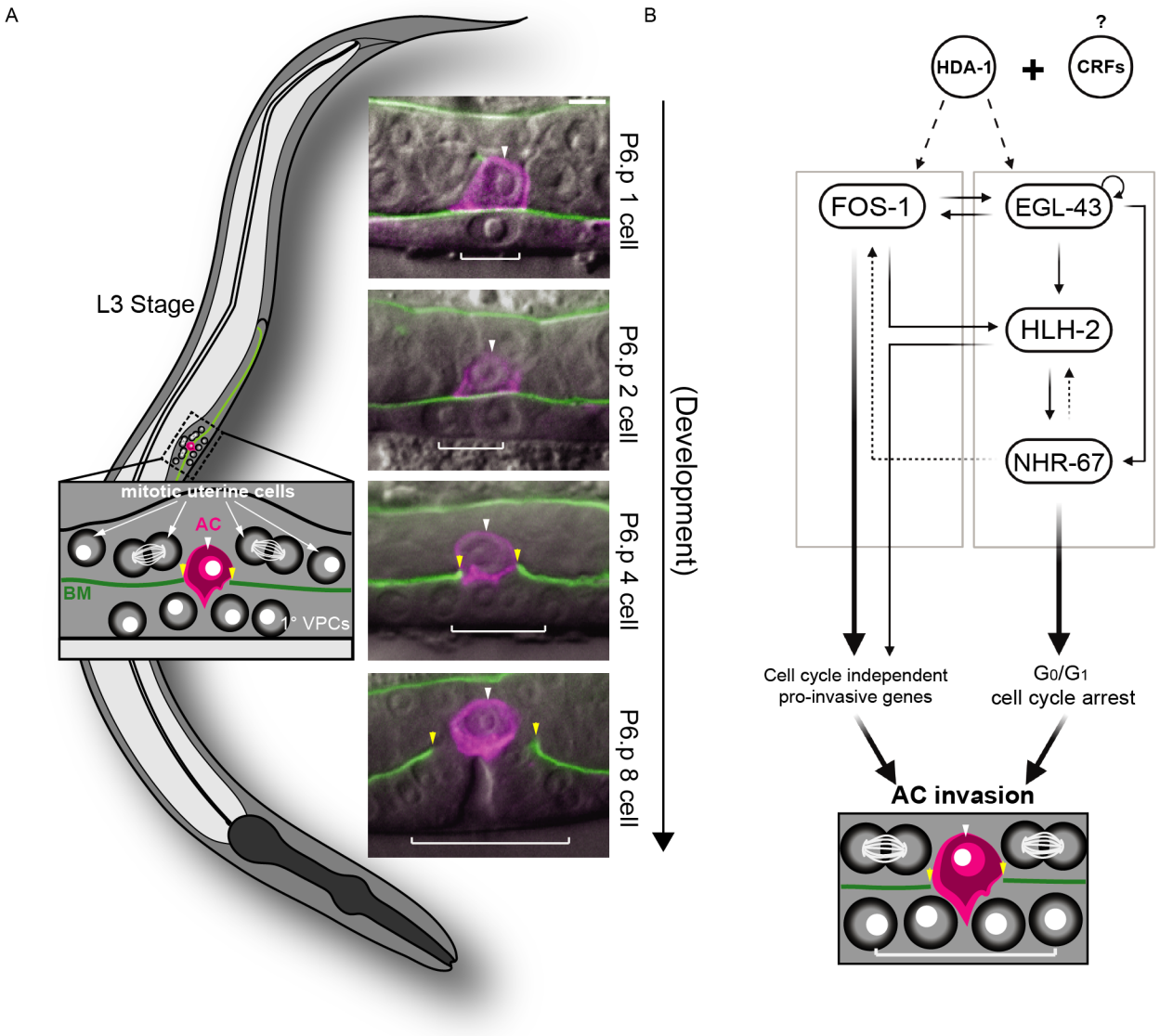

Figure 1. Summary of *C. elegans* AC invasion through the underlying BM and AC GRN. (A) Schematic depicting AC invasion in the mid-L3 stage of *C. elegans* development (left) and micrographs demonstrating the coordination of AC (magenta, *cdh-3p::PH::mCherry*) invasion through the BM (green, *laminin::GFP*) with primary vulval development. The fluorescent AC-specific membrane marker and BM marker are overlaid on DIC in each image. White arrowheads indicate AC(s), yellow arrowheads indicate boundaries of breach in BM, and white brackets indicate 1° VPCs. **(B)** Overview of the transcription factor GRN governing AC invasion (22,24), which consists of cell cycle-independent (*fos-1*) and dependent (*egl-43, hlh-2,* and *nhr-67*) subcircuits, which together with *hda-1* promote pro-invasive gene expression and maintain cell cycle arrest in the AC. In this and all subsequent figures, scale bar, 5 μm.

Previous work demonstrated a high degree of evolutionary conservation in the cell-autonomous mechanisms underlying BM invasion (3,15), including basolateral polarization of the F-actin cytoskeleton/cytoskeletal regulators and the expression of

84 matrix metalloproteinases (MMPs) (16–21). Moreover, in order to breach the BM, the AC
85 requires the expression of transcription factors (TFs), whose human homologs are
86 common to metastatic cancers, including *egl-43* (EVI1/MEL), *fos*-1 (FOS), *hlh-2*
87 (E/Daughterless), and *nhr-67* (TLX/Tailless) (22) (**Fig 1 B**). In addition to the expression
88 of pro-invasive genes, there is increasing evidence that cells must also arrest in the cell
89 cycle to adopt an invasive phenotype (23). Our previous work has demonstrated that the
90 AC must terminally differentiate and arrest in the G_0/G_1 phase of the cell cycle to invade
91 the BM and make contact with the underlying primary vulval precursor cells (1° VPCs)
92 (22,24). The regulatory mechanisms that couple G_0/G_1 cell cycle arrest with the ability of
93 a cell to invade the BM remain unclear.

94 Cell-extrinsic and cell-intrinsic factors, such as chromatin remodeling complexes
95 and TFs, can influence the decision to maintain a plastic cell fate or to undergo cell fate
96 specification and terminal differentiation. The determination of a cell to remain plastic or
97 specify is in part the consequence of a complex, genome-wide antagonism between
98 Polycomb group (PcG) transcriptional repression and Trithorax group (TrxG)
99 transcriptional activation (25–27). For example, the binding of pioneer transcription
100 factors OCT4 and SOX2 to target DNA in order to retain pluripotency in murine embryonic
101 stem cells is the indirect consequence of the regulation of chromatin accessibility at these
102 target regions (28). A recent study has shown that chromatin accessibility of enhancers
103 in crucial cell cycle genes which promote the G_1/S transition, including Cyclin E and E2F
104 transcription factor 1, is developmentally restricted to reinforce terminal differentiation and
105 cell cycle exit during *Drosophila melanogaster* pupal wing morphogenesis (29). In *C.*
106 *elegans* myogenesis, the SWItching defective/Sucrose Non-Fermenting (SWI/SNF) ATP-

107 dependent chromatin remodeling complex, a member of the TrxG family of complexes,
108 both regulates the expression of the MyoD transcription factor (*hlh-1*) and acts
109 redundantly to promote differentiation and G_0 cell cycle arrest with core cell cycle
110 regulators: cullin 1 (CUL1/*cul-1)*, cyclin-dependent kinase inhibitor 1 (*cki-1)*, FZR1 (*fzr*-1),
111 and the RB transcriptional corepressor (RBL1/*lin*-35). The importance of regulation of
112 chromatin states and the activity of CRFs for the acquisition and implementation of
113 differentiated behaviors is also reflected in the *C. elegans* AC, as previous work has
114 shown that the histone deacetylase *hda-1* (HDAC1/2) is required for pro-invasive gene
115 expression and therefore differentiated cellular behavior and invasion (24) (**Fig 1 B**).
116 Given these findings, a comprehensive investigation of the regulatory mechanism(s)
117 governing AC invasion should include a thorough description of the suite of CRFs
118 required for G_0/G_1 cell cycle arrest and invasive differentiation in the AC.

119 In this study we perform an RNA interference (RNAi) screen of *C. elegans* CRFs,
120 specifically focusing on genes involved in chromatin structure and remodeling or histone
121 modification. We identify 82 genes whose RNAi depletion phenotype resulted in a
122 significant AC invasion defect. Among the CRFs identified as significant regulators of AC
123 invasion, the SWI/SNF complex emerged as the most well-represented single chromatin
124 remodeling complex. RNAi knockdown of subunits specific to the SWI/SNF core (*swsn-1*
125 and *snfc-5/swsn-5*), and both BAF (BRG/BRM-Associated Factors; *swsn-8/let-526*) and
126 PBAF (Polybromo Associated BAF; *pbrm-1* and *swsn-7*) assemblies resulted in penetrant
127 loss of AC invasion. We generated fluorescent reporter knock-in alleles of subunits of the
128 core (*GFP::swsn-4*) and BAF (*swsn-8::GFP*) assembly of the SWI/SNF complex using
129 CRISPR/Cas9-mediated genome engineering. These alleles, used in conjunction with an

130 endogenously labeled PBAF (*pbrm-1::eGFP*) assembly subunit, enabled us to determine
131 the developmental dynamics of the SWI/SNF ATPase and assembly-specific subunits,
132 gauge the efficiency of various SWI/SNF knockdown strategies, and asses inter- and
133 intra-complex regulation. Using improved RNAi constructs and an anti-GFP nanobody
134 degradation strategy (30), we demonstrated that the cell autonomous contribution of the
135 SWI/SNF complex to AC invasion is dose dependent. This finding parallels similar studies
136 in cancer (31–34) and *C. elegans* mesoblast development (35). Examination using a CDK
137 activity sensor (36) revealed assembly-specific contributions to AC invasion: whereas
138 BAF promotes AC invasion in a cell cycle-dependent manner, PBAF contributes to
139 invasion in a cell cycle-independent manner. Finally, we utilized the auxin-inducible
140 degron (AID) system combined with PBAF RNAi to achieve strong PBAF subunit
141 depletion in the AC, which resulted in loss of both AC invasion and adhesion to the BM.
142 Together, these findings provide insight into how the SWI/SNF complex assemblies may
143 contribute to distinct aspects of proliferation and metastasis in human malignancies.
144

145 **RESULTS**

146 **An RNAi screen of 269 CRFs identified SWI/SNF as a key regulator of AC invasion**

147 To identify the suite of CRFs that, along with *hda-1,* contribute to AC invasion, we
148 generated an RNAi sub-library of 269 RNAi clones from the complete Vidal RNAi library
149 and a subset of the Ahringer RNAi library (37,38) targeting genes implicated in chromatin
150 state, chromatin remodeling, or histone modification (**Table S1**) (**Fig 1 B**). Because CRFs
151 act globally to control gene expression, we screened each RNAi clone by high-resolution
152 differential interference contrast (DIC) and epifluorescence microscopy in a uterine-

153 specific RNAi hypersensitive background containing labeled BM (*laminin::GFP*) and an
154 AC reporter (*cdh-3p::PH::mCherry*) (**Fig 1 A; Table S1**) (14,22,24,39). This genetic
155 background allowed us to limit the effect of transcriptional knockdown of CRFs to only
156 affect the AC and the neighboring uterine tissue, and only for a time period following the
157 specification of the AC (39). As the neighboring uterine cells do not contribute to the
158 invasion program (14), AC invasion defects following RNAi treatments are indicative of
159 cell autonomous pro-invasive gene function (24,39). In wild-type animals, by the time the
160 1˚ fated P6.p vulval precursor cell has divided twice (P6.p 4-cell stage), 100% of ACs
161 have successfully breached the underlying BMs and made contact with the P6.p grand-
162 daughters (14). While the AC also always invades in the uterine-specific RNAi
163 hypersensitive strain we utilized for our CRF screen, there is a low penetrance delay,
164 such that at the P6.p 4-cell stage, when we scored invasion, 2% (2/100 animals) still had
165 an intact BM. Thus, we used this baseline defect as a statistical reference point for this
166 genetic background and defined the cut-off threshold for significant defects in invasion
167 from RNAi depletion of CRFs in our screen as those RNAi clones that resulted in a ~13%
168 or greater defect in invasion (4/30 animals, Fisher's exact test = 0.0252). By this
169 threshold, we recovered 82 CRFs (30.5% of total CRFs screened) that significantly
170 regulate AC invasion, suggesting a general role for regulation of chromatin states in the
171 acquisition of invasive behavior (**Table S2**). Interestingly, five subunits of the broadly
172 conserved SWI/SNF chromatin remodeling complex were recovered as significant
173 regulators of AC invasion: *swsn-1*(SMARCC1/SMARCC2; 23% AC invasion defect),
174 *swsn-5/snfc-5* (SMARCB1; 20% AC invasion defect), *swsn-7* (ARID2; 23% AC invasion
175 defect), *swsn-8/let-526* (ARID1A/ARID1B; 23% AC invasion defect), and *pbrm-1*

176 (PBRM1; 20% AC invasion defect) (**Table S2**). As such, SWI/SNF is well-represented in
177 our CRF screen, with representation of the core (*swsn-1* and *swsn-5*), BAF (*swsn-8*) and
178 PBAF (*pbrm-1* and *swsn-7*) assemblies. Given the prevalence of SWI/SNF subunits
179 recovered as significant regulators of AC invasion in our RNAi screen and the crucial role
180 SWI/SNF plays in the regulation of animal development (40–45), tumorigenesis (32,46–
181 48), and cell cycle control (35,49–52), we chose to focus our efforts on characterizing the
182 role of the SWI/SNF complex in promoting AC invasion.

183 To confirm our RNAi results implicating the SWI/SNF complex in the promotion of
184 AC invasion, we obtained two temperature sensitive hypomorphic alleles, *swsn-1(os22)*
185 and *swsn-4(os13)* (41), and scored for defects in AC invasion in a genetic background
186 containing both BM (*laminin::GFP*) and AC (*cdh-3p::mCherry::moeABD*) reporters. While
187 we observed no defects in AC invasion in animals grown at the permissive temperature
188 (15°C) (**Fig S1 A**), animals containing hypomorphic alleles for core subunits *swsn-1* and
189 *swsn-4* cultured at the restrictive temperature (25°C) displayed defects in 20% (10/50)
190 and 24% (12/50) of animals, respectively. These results with the *swsn-1(os22)* allele
191 corroborated our *swsn-1(RNAi)* data from the CRF RNAi screen. Since neither of the
192 RNAi libraries used to compose the CRF screen (see above) contained a *swsn-4(RNAi)*
193 clone, results with the *swsn-4(os13)* allele also supplement data from our CRF RNAi
194 screen by suggesting that AC invasion depends on the expression of the sole *C. elegans*
195 SWI/SNF ATPase subunit in addition to the 5 subunits identified in the screen (**Fig S1 B**).
196

197 **Improved RNAi vectors revealed distinct contributions of SWI/SNF subunits to AC**
198 **invasion**

199 Though many SWI/SNF assemblies have been described in mammalian and other
200 systems, including BAF, PBAF, esBAF, GBAF, nBAF, and npBAF) (53), to date, BAF and
201 PBAF are the only SWI/SNF assemblies that have been described in *C. elegans*. Both
202 assemblies consist of core subunits (SWSN-1, SWSN-4, SWSN-5) and accessory
203 subunits (DPFF-1, SWSN-2.1/HAM-3, SWSN-2.2, SWSN-3, SWSN-6, and PHF-10),
204 collectively referred to as common factors (46,54). These common factors are bound by
205 assembly-specific subunits in a mutually exclusive manner, which confers the distinct
206 character of each of the two assemblies (**Fig 2 A**). Due to the absence of thorough
207 biochemical investigation into the SWI/SNF complex in *C. elegans*, previous publications
208 have classified subunits as part of the SWI/SNF core, accessory, or BAF/PBAF
209 assemblies based on homology and phenotypic analyses (35,43,52,55). The prevailing
210 model for the two SWI/SNF assemblies in *C. elegans* is that either the SWSN-8 subunit
211 associates with common factors to form the BAF assembly, or the SWSN-7, SWSN-9,
212 and PBRM-1 subunits associate with common factors to form the PBAF assembly
213 (43,55,56). Prior investigations into SWI/SNF have revealed a wide array of
214 developmental contexts in which the BAF and PBAF assemblies have overlapping and
215 distinct roles in the regulation of cell cycle control, differentiation, and differentiated
216 behavior (35,52,55,57–61).

217 To investigate the contribution of individual SWI/SNF subunits to AC invasion and
218 to distinguish potentially distinct roles of the BAF and PBAF assemblies, we generated
219 improved RNAi constructs utilizing the T444T vector (62) to target representative subunits
220 of the core and both SWI/SNF assemblies (**Table S3**). Knockdown of SWI/SNF subunits
221 in whole-body RNAi sensitive animals following treatment with T444T RNAi vectors

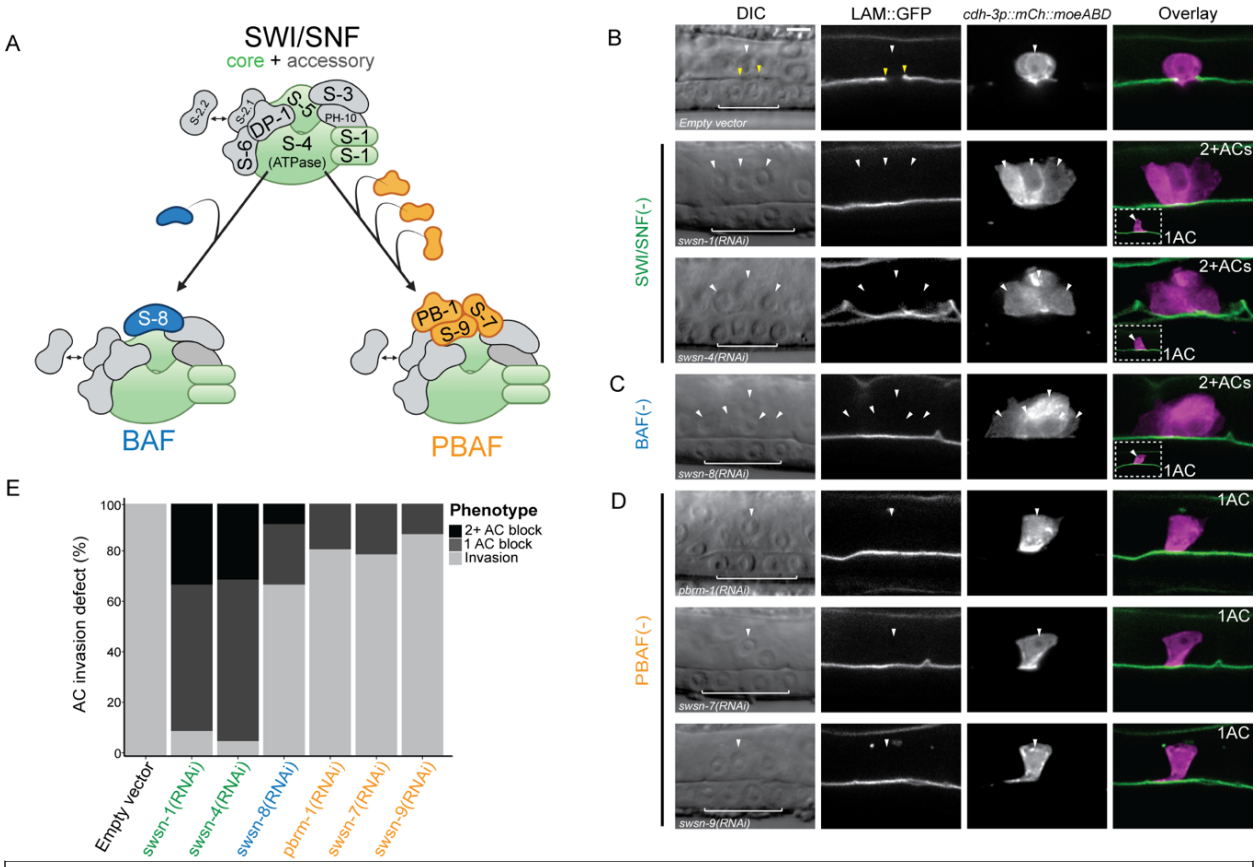

Figure 2. Enhanced RNAi targeting SWI/SNF core, BAF, and PBAF assembly subunits results in penetrant invasion defects. (A) Schematic depicting the *C. elegans* SWI/SNF core (middle, green) and accessory (middle, gray) subunits and BAF (left, blue), and PBAF (right, orange) assemblies. **(B-D)** DIC (left), corresponding fluorescence images (middle), and fluorescence overlay (right) representing loss of AC (magenta, *cdh-3p::mCherry::moeABD*) invasion through the BM (green, *laminin::GFP*) following RNAi depletion of SWI/SNF core (*swsn-1* and *swsn-4*) **(B)**, BAF (*swsn-8*) **(C)**, and PBAF (*pbrm-1, swsn-7,* and *swsn-9*) **(D)** subunits. In cases where multiple cells expressed the AC reporter (2+ACs) in the same animal, each is indicated with a white arrowhead. In cases where multiple cells expressed the AC reporter (2+ACs), a representative image from the same treatment of a single AC that fails to breach the BM is displayed as an inset (white dashed box, bottom left). White arrowheads indicate AC(s), yellow arrowheads indicate boundaries of breach in BM, and white brackets indicate 1° VPCs. **(E)** Stacked bar chart showing the penetrance of AC invasion defects following treatment with SWI/SNF RNAi depletion, binned by AC phenotype (n≥50 animals examined for each treatment).

222 resulted in penetrant loss of invasion. The majority of ACs failed to invade following
223 treatment with RNAi targeting the core SWI/SNF ATPase subunit *swsn-4* or core subunit
224 *swsn-1* (90% and 94%, respectively; n=50 animals; **Fig 2 B, E**). RNAi-mediated
225 knockdown of the BAF assembly subunit *swsn-8* also resulted in significant loss of AC
226 invasion (32%; n=50 animals; **Fig 2 C, E**). Knockdown of the PBAF assembly subunits

227 with *pbrm-1(RNAi), swsn-7(RNAi)*, or *swsn-9(RNAi)* resulted in a less penetrant loss of
228 AC invasion (18%, 20%, and 12%, respectively; n=50 animals; **Fig 2 D, E**). Importantly,
229 at least one cell in the ventral uterus expressed the fluorescent AC reporter in all animals
230 across all treatments, suggesting that loss of the SWI/SNF complex does not preclude
231 the birth of an AC.

232 Interestingly, in addition to a single non-invasive AC phenotype, RNAi-mediated
233 knockdown of *swsn-1*, *swsn-4* or *swsn-8* also resulted in a second phenotype
234 characterized by multiple uterine cells expressing the AC reporter (*cdh-*
235 *3p::mCherry::moeABD*) which failed to invade the BM (*laminin::GFP*) (32%, 30% and 8%,
236 respectively; **Fig 2 B-C, E**). In all instances where more than one cell expressed the AC
237 reporter, no breach in the underlying BM was detected at the P6.p 4-cell stage. In
238 contrast, only the single non-invasive AC phenotype resulted from RNAi treatment
239 targeting PBAF assembly subunits (**Fig 2 D-E**). These results suggest that the SWI/SNF
240 assemblies BAF and PBAF may promote AC invasion through distinct mechanisms,
241 perhaps via regulation of both a cell cycle-dependent and -independent mechanism,
242 respectively.

243

244 **Characterization of endogenous GFP reporter alleles and the efficacy of improved**
245 **SWI/SNF RNAi vectors**

246 Next, to confirm expression of SWI/SNF subunits in the AC and to quantitatively
247 assess the potency of our enhanced SWI/SNF RNAi vectors we utilized CRISPR/Cas9
248 genome engineering to generate GFP-tagged alleles of *swsn-4* and *swsn-8*, inserting a
249 codon-optimized GFP tag into the 5' end and 3' end of the *swsn-4* and *swsn-8* loci,

250 respectively (**Fig S2 A**) (63). The GFP-tagged endogenous strains showed ubiquitous
251 and nuclear-localized expression of GFP::SWSN-4 and SWSN-8::GFP throughout the *C.*
252 *elegans* developmental life cycle (**Fig S2 B**). We also obtained a strain containing an
253 endogenously eGFP-labeled PBAF subunit (*pbrm-1::eGFP*) from the *Caenorhabditis*
254 Genetics Center (CGC). We quantified fluorescence protein expression of SWI/SNF core
255 ATPase (GFP::SWSN-4), BAF (SWSN-8::GFP), and PBAF (PBRM-1::eGFP) subunits in
256 the AC during vulval development across the L3 and early L4 stages, as defined by the
257 division pattern of the 1°-fated VPCs (14) (n≥28 animals per stage; **Fig S3 A-C'**).
258 Expression of all three subunits was enhanced in the AC relative to the neighboring
259 ventral uterine (VU; *swsn-4*: 18%, *swsn-8*: 21%, *pbrm-1*: 17% enhanced) and 1° VPC
260 (*swsn-4*: 30%, *swsn-8*: 38%, *pbrm-1*: 23% enhanced) lineages during AC invasion (P6.p
261 2 cell – 4 cell stage, **Fig S3 A'-C'**). Late in vulval development at the P6.p 8 cell stage,
262 expression of GFP::SWSN-4 and PBRM-1::eGFP increases in the 1° VPCs and is no
263 longer statistically separable from expression in the AC, whereas expression of SWSN-
264 8::GFP in the VPCs remains significantly lower than in the AC (**Fig S3 A'-C'**).

265 We treated SWI/SNF endogenously labeled GFP-tagged strains with our RNAi
266 vectors to precisely quantify the efficiency of RNAi-mediated knockdown of target
267 SWI/SNF complex subunits and to correlate this loss with the resulting AC phenotypes.
268 Treatment with either *swsn-4(RNAi)* or *swsn-8(RNAi)* vectors resulted in robust depletion
269 of fluorescence expression of GFP::SWSN-4 (94% depletion) and SWSN-8::GFP (81%
270 depletion) in the AC (**Fig S4 A-B, D**) and penetrant loss of invasion (90% and 30%,
271 respectively; n=30 animals for each condition; **Fig S4 E**). We also noted instances where
272 multiple cells expressed the AC reporter (23% and 10%, respectively; n=30 animals for

273 each condition; **Fig S4 E**). Treatment of the PBRM-1::eGFP strain with *pbrm-1(RNAi)*
274 revealed weaker but significant knockdown of PBRM-1 protein (49% depletion), and a
275 lower penetrance of invasion defects (17%; n=30 animals; **Fig S4 C-E**). It is unclear why
276 PBRM-1::eGFP endogenous protein level in the AC of animals treated with enhanced
277 *pbrm-1(RNAi)* remains considerably higher compared to treatment of strains containing
278 *swsn-4* or *swsn-8* reporter alleles with their respective RNAis. We hypothesize that this
279 may be the consequence of differential protein perdurance. Altogether, these results
280 confirm the dynamic expression of the SW/SNF core, BAF, and PBAF subunits in the AC
281 before, during, and after invasion and demonstrate the effectiveness of our improved
282 SWI/SNF-targeting RNAi vectors.
283

284 ***C. elegans* SWI/SNF subunits exhibit low levels of intracomplex cross-regulation**

285 Work in mammalian cell culture has revealed that the mSWI/SNF complex is
286 assembled in a step-wise fashion, with stability of the complex as a whole and association
287 of individual subunits depending on the prior expression and association of other subunits
288 (64)**.** To date it is unknown whether in *C. elegans* individual SWI/SNF subunits activate
289 other SWI/SNF subunits. It is also unclear whether subunits of the two assemblies in *C.*
290 *elegans* – BAF and PBAF – stabilize the core protein subunits or vice-versa. Therefore,
291 we used our endogenously labeled GFP-SWI/SNF strains to ask whether transcriptional
292 knockdown of individual subunits of the core, BAF, or PBAF induce changes in protein
293 expression of other subunits at the time of AC invasion (**Fig S5**). First, to determine
294 whether representative subunits of the SWI/SNF assemblies promote or stabilize the
295 ATPase of the complex, we treated *GFP::swsn-4* animals with either *swsn-8(RNAi)* or

296 *pbrm-1(RNAi)* (**Fig S5 A**). Quantification of fluorescence expression in AC nuclei of *swsn-*
297 *8(RNAi)* treated animals at the P6.p 4 cell stage revealed significantly lower GFP::SWSN-
298 4 levels relative to the control group (34% GFP::SWSN-4 depletion; **Fig S5 A, D**). RNAi
299 knockdown of the PBAF subunit *pbrm-1* also resulted in a significant but weaker loss of
300 ATPase expression in the AC (11% GFP::SWSN-4 depletion; **Fig S5 A, D**). These results
301 suggest that individual subunits of either SWI/SNF assembly may contribute to the protein
302 stability and/or expression of the SWI/SNF ATPase in the *C. elegans* AC, with the BAF
303 complex playing a potentially dominant activating role with respect to the ATPase.

304 Next, we treated animals containing either the *swsn-8* or *pbrm-1* endogenous
305 GFP-reporters with enhanced RNAi to knockdown the expression of the SWI/SNF
306 ATPase or the representative subunit of the alternative SWI/SNF assembly. Interestingly,
307 while unaffected by knockdown of the PBAF assembly subunit *pbrm-1,* RNAi knockdown
308 of the ATPase *swsn-4* resulted in a 42% increase in the expression of SWSN-8::GFP in
309 the AC (**Fig S5 B, D**). Finally, relative to the expression of the endogenous PBAF subunit
310 in the ACs of animals treated with the empty vector control RNAi, AC nuclei of PBRM-
311 1::eGFP animals treated with *swsn-4(RNAi)* had significantly lower levels of protein
312 expression (38% PBRM-1::eGFP depletion), whereas ACs in *swsn-8(RNAi)* treated
313 animals expressed 13% more PBRM-1::eGFP (**Fig S5 C-D**).

314 Since knockdown of either *swsn-4* or *swsn-8* subunits resulted in two distinct
315 phenotypes – individual animals with single non-invasive ACs and animals with multiple
316 non-invasive cells expressing the AC-reporter - we next sought to determine whether
317 these two phenotypes were distinct with respect to SWI/SNF subunit expression. To do
318 this, we binned data from the intracomplex RNAi experimental series (above) into the two

319 non-invasive phenotypes and compared the fluorescence expression levels of the
320 endogenous proteins within SWI/SNF RNAi conditions. Given the infrequency of the
321 multi-AC phenotype, statistical comparisons were necessarily limited to treatments in
322 which the population of animals contained at least 10 multi non-invasive ACs. Treatment
323 of SWSN-8::GFP with *swsn-4(RNAi)* resulted in a total of 24 multi non-invasive ACs (53
324 ACs total; n=41 animals) and no significant difference was detected in SWSN-8::GFP
325 expression between the nuclei of the single non-invasive AC phenotype and the multi
326 non-invasive AC phenotype groups (**Fig S5 E**). The second statistical comparison was
327 made between the two phenotypes in PBRM-1::eGFP animals treated with *swsn-8(RNAi)*
328 (**Fig S5 E**), in which 14 multi non-invasive ACs were detected (51 ACs total; n=42
329 animals). Quantification of endogenous PBRM-1::eGFP fluorescence expression in this
330 condition revealed a slight (12%) increase in expression of the PBAF subunit in the nuclei
331 of ACs of the multi non-invasive phenotype group compared to the single non-invasive
332 phenotype (**Fig S5 E**).

333 Based on these results, a tentative model for epistatic interactions between the
334 SWI/SNF ATPase, BAF, and PBAF assembly subunits can be composed for the AC (**Fig**
335 **S5 F)**. Our data indicate that some degree of SWI/SNF intra- and inter-complex regulation
336 occurs in the AC. We find that the most significant aspect of SWI/SNF intra-complex
337 regulation is exercised by the ATPase on the assembly specific subunits, where *swsn-4*
338 knockdown results in a significant increase in BAF/SWSN-8 and a significant decrease
339 PBAF/PBRM-1. SWI/SNF intercomplex regulation appears to be weaker in the AC as
340 knockdown of *pbrm-1* does not affect SWSN-8::GFP expression, and knockdown of
341 *swsn-8* results in a slight increase in PBRM-1::GFP expression.

342

343 **The SWI/SNF ATPase SWSN-4 provides dose-dependent regulation of AC invasion**

344 The degree to which the SWI/SNF complex contributes to tumorigenesis in clinical
345 settings has been linked to the dose of functional SWI/SNF ATPase in precancerous and
346 transformed cells (32,34,65). Previous work in *C. elegans* has demonstrated a similar
347 dose dependent relationship between SWI/SNF and cell cycle control (35). To determine
348 whether the phenotypic dosage sensitivity seen in cancer and *C. elegans* mesodermal
349 (M) cell development is also characteristic of SWI/SNF in the promotion of AC invasion
350 (30), we modulated expression of GFP::SWSN-4 using a combination of RNAi-mediated
351 knockdown and AC-specific GFP-targeting nanobody technology.

352 Though RNAi treatment targeting the *swsn-4* subunit in the endogenously-tagged
353 strain resulted in significant knockdown of fluorescence expression of GFP::SWSN-4 in
354 the AC, loss of expression was noted in many other tissues in treated animals, including
355 the 1° VPCs, which contribute to AC invasion non-autonomously (14,66) (**Fig S4**). Thus,
356 to limit loss of expression to the AC, we used an anti-GFP nanobody fused to a SOCS-
357 box containing a ubiquitin ligase adaptor, driven with tissue-specific promoters to achieve
358 lineage-restricted protein depletion (30) (**Fig 3**). To follow the expression of the anti-GFP
359 nanobody transgenes, we also included a fluorescent histone label separated from the
360 anti-GFP nanobody sequence by the p2a viral self-cleaving peptide (*ACp::antiGFP-*
361 *nanobody::p2a::His-58::mCherry*). We generated two anti-GFP nanobody constructs,
362 using conserved *cis*-regulatory elements from the *cdh-3* and *egl-43* promoters
363 (22,24,39,67,68) and introduced them into a strain containing the endogenous GFP-
364 tagged allele of *swsn-4* as well as background AC and BM reporters (**Fig 3 B-C**). The

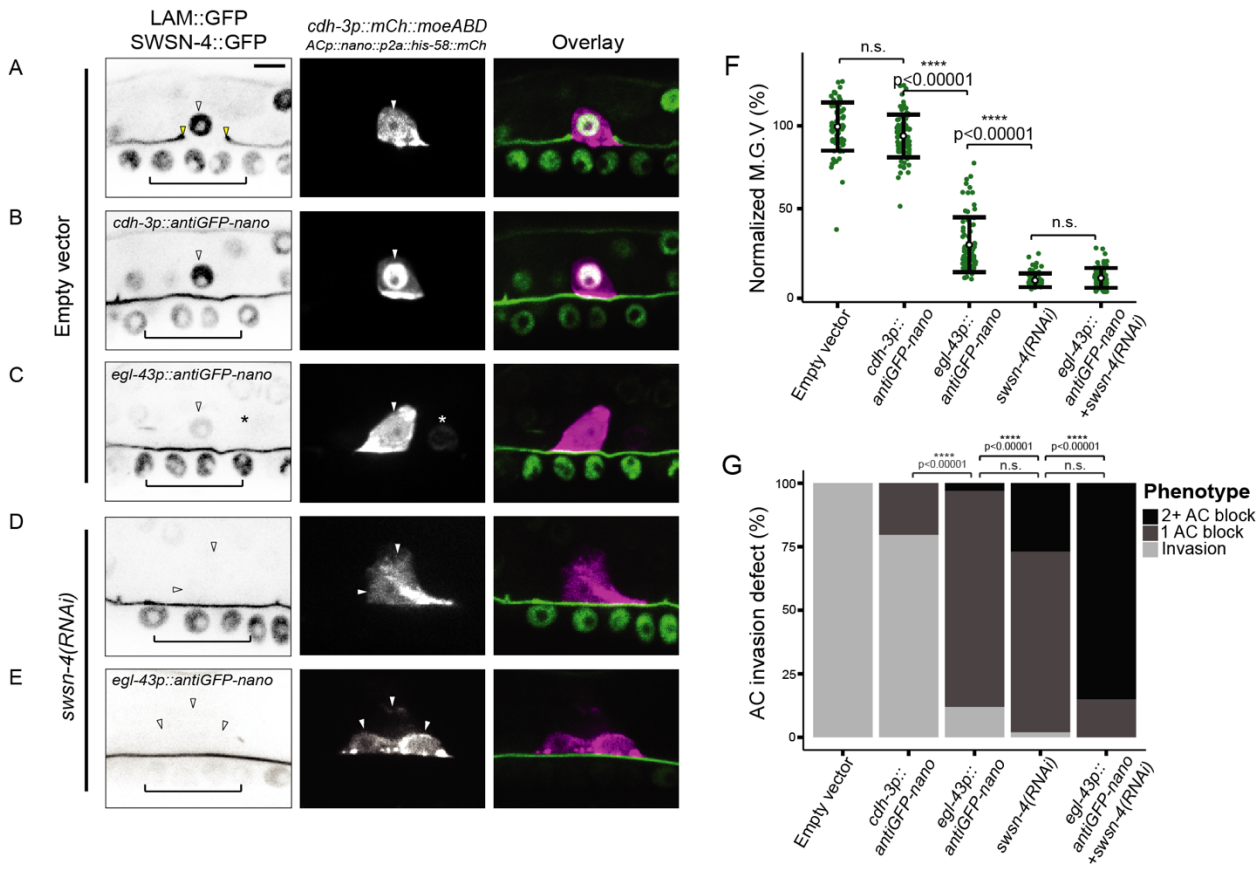

Figure 3. AC invasion and cell cycle arrest depend on dosage of SWI/SNF ATPase. (A-E) Representative fluorescence images depicting expression of BM marker (*laminin::GFP*) and endogenous GFP::SWSN-4 (left), AC reporter (*cdh-3p::mCherry::moeABD*, middle), and fluorescence overlay (right) across experimental treatments. White arrowheads indicate AC(s), yellow arrowheads indicate boundaries of breach in BM, and black brackets indicate 1° VPCs. In cases where multiple cells expressed the AC reporter in the same animal, each is indicated with a single white arrowhead. Asterisk indicates anti-GFP nanobody expression in neighboring VU cell. **(F)** Quantification of mean gray values (M.G.V.) of endogenous GFP::SWSN-4 in ACs in control animals (empty vector) and across all experimental treatments normalized to mean fluorescent expression in wildtype animals (n≥40 animals per treatment, p values for Student's *t*-test comparing expression of successive knockdown are displayed on the figure). In this and all other figures, open circles and error bars denote mean±standard deviation (s.d.). n.s. not significant. **(G)** Stacked bar chart showing quantification of AC invasion defects corresponding to each treatment, binned by AC phenotype (n≥40 animals per condition; p values for Fisher's exact test comparing phenotypes of successive knockdown strategies are displayed above compared groups). Grey brackets indicate statistical significance between invasion total in each condition compared to invasion defect total. Black brackets indicate statistical significance between incidences of invasion defects with multiple ACs compared to incidences of invasion defects with single ACs. n.s. not significant.

365 *cdh-3*-driven nanobody transgene (*cdh-3p::antiGFP-nanobody::p2a::his-58::mCherry*)
366 resulted in a weak reduction of GFP::SWSN-4 levels with no significant difference in
367 fluorescence expression in the AC compared to wildtype animals (6% depletion; n=80

368 animals; **Fig 3 F**); however, consistent with the wildtype expression of the *cdh-3* promoter
369 (22,39), it expressed specifically in the AC and resulted in defective AC invasion,
370 suggesting partial loss of function (20.6% AC invasion defect; n=102; **Fig 3 B, G**). The
371 *egl-43p::antiGFP-nanobody* transgene (*egl-43p::antiGFP-nanobody::p2a::His-*
372 *58::mCherry*) expression pattern was also consistent with the wildtype expression
373 characterized in previous work (22,67–69), as indicated by nuclear expression of HIS-
374 58::mCherry in the AC and in the neighboring ventral uterine and dorsal uterine (VU/DU)
375 cells (**Fig 3 C**; asterisk denotes HIS-58::mCherry expression in a non-AC ventral uterine
376 cell) (22,39,67). Importantly, as the AC invades independent of VU/DU cells (14), anti-
377 GFP expression in these tissues should not affect AC invasion. Similar to animals treated
378 with *swsn-4(RNAi)* (**Fig 3 D**), *egl-43p::antiGFP-nanobody*-mediated protein depletion of
379 GFP::SWSN-4 resulted in a significant loss of fluorescence expression in the AC (71%
380 GFP depletion; n=80 animals; **Fig 3 C, F**) as well as a penetrant loss of invasion and
381 incidence of individual animals with multiple uterine cells that were in contact with the
382 ventral BM and expressed the AC reporter (88.2% AC invasion defect, 2.9% multiple AC
383 phenotype; n=101 animals; **Fig 3 G**). These results support our uterine-specific SWI/SNF
384 RNAi results and provide strong evidence for a cell-autonomous role for the SWI/SNF
385 complex in promoting cell invasion and cell cycle arrest.

386 To further deplete *swsn-4* expression in the AC, we treated transgenic *egl-*
387 *43p::antiGFP-nanobody* animals with *swsn-4(RNAi)* (**Fig 3 E**). Strikingly, in this
388 combination knockdown strategy, 100% of AC invasion was lost and the frequency of
389 multiple cells expressing the AC specification reporter drastically increased relative to
390 treatment with *swsn-4(RNAi)* or the *egl-43*-driven anti-GFP nanobody conditions alone

391 (83% multiple AC phenotype; n=41 animals; **Fig 3 G**). Together, these results
392 demonstrate a phenotypic spectrum that corresponds to successive loss of *swsn-4* in the
393 AC: whereas moderate loss of the ATPase results in single non-invasive ACs in animals
394 containing *egl-43p::antiGFP-nanobody*, strong loss of expression in the *egl-*
395 *43p::antiGFP-nanobody* background or following treatment with *swsn-4(RNAi)* results in
396 animals with both single and multiple non-invasive ACs; in the strongest knockdown
397 condition – *egl-43p::antiGFP-nanobody* animals treated with *swsn-4(RNAi)* - multiple
398 non-invasive ACs were present per animal with near complete penetrance. Though the
399 combination of *swsn-4(RNAi)* and antiGFP-nanobody-mediated depletion resulted in
400 robust loss of expression of the core ATPase of the SWI/SNF complex, the fluorescence
401 expression was not significantly different than treatment with *swsn-4(RNAi)* alone (93%
402 vs. 92% GFP depletion, respectively; n≥41 animals for each treatment; **Fig 3 G**); therefore
403 we theorize that the fluorescence values were beyond our threshold ability to quantify
404 based on the fluorescence detection limits of our imaging system. Altogether, our data
405 demonstrated that in the AC, the ATPase of the SWI/SNF complex contributes to invasion
406 cell-autonomously and in a dose-dependent manner: moderate loss of expression
407 produced non-invasive single ACs while extreme loss of expression led to a non-invasive
408 hyperproliferative state.
409

410 **Improved *swsn-4(RNAi)* vector is sufficient to recapitulate null phenotype in M**
411 **lineage**

412 A recent study focusing on cell cycle control of SWI/SNF throughout *C. elegans*
413 muscle and epithelial differentiation demonstrated tissue and lineage-specific phenotypes

414 following weak or strong loss of core SWI/SNF subunits (32). Within the M lineage that
415 gives rise to posterior body wall muscles (BWMs), coelomocytes (CCs), and reproductive
416 muscles or sex myoblast (SMs) descendants, different cell types responded differently to
417 loss of SWI/SNF. In the BWM, strong loss of SWI/SNF resulted in hyperproliferation, like
418 the phenotype we detect in the AC. The opposite is true in the SM lineage, where modest
419 knockdown of *swsn-4* resulted in hyperproliferation while complete loss of *swsn-4*
420 expression resulted in a null phenotype where SMs failed to divide and arrest in S phase
421 (35). We next sought to validate the strength of our enhanced *swsn-4(RNAi)* vector by
422 examining proliferative state in the SMs. To accomplish this, we treated animals
423 containing a lineage-restricted cyclin-dependent kinase (CDK) activity sensor (*unc-*
424 *62p::DHB::2xmKate2*) with *swsn-4(RNAi)* (**Fig S6 A**). In this genetic background, we
425 determined the number (**Fig S6 B**) and cell cycle state (**Fig S6 C**) of SM cells at a time
426 when the majority of SMs in control animals had finished cycling and subsequently
427 differentiated (late P6.p 8 cell stage; 16 SM cell stage). Animals treated with *swsn-*
428 *4(RNAi)* had significantly fewer SM cells than controls (mean SMs/animals = 5; n=31
429 animals; **Fig S6 B**) with many instances of SMs that failed to enter a single round of cell
430 division (n=20 single SMs out of 43 animals). Interestingly, 28% (12/43) of animals treated
431 with *swsn-4(RNAi)* were absent of SMs on either the left or the right side, whereas 100%
432 (30/30) control animals had SMs on both sides, which may indicate a defect in
433 specification, early cell division, and/or migration of SMs. To quantify cell cycle state, we
434 measured localization of an SM-specific CDK sensor, which uses a fragment of
435 mammalian DNA Helicase B (DHB) fused to two copies of mKate2 (36,70). In cells with
436 low CDK activity that are quiescent or post-mitotic, the ratiometric CDK sensor is strongly

437 nuclear localized (36,68,70). In cycling cells with increasing CDK activity, the CDK sensor
438 progressively translocates from the nucleus to the cytosoplasm, with a ratio approaching
439 1.0 in S phase and >1 in cells in G_2 (36). Thus, the cytoplasmic:nuclear (C/N) ratio of
440 DHB::2xmKate2 can serve as a proxy to identify cell cycle state. By the time the majority
441 of SMs in the control condition were differentiating and arrested in a G_0 cell cycle state
442 (mean C/N ratio=0.320; n=90 SMs; **Fig S6 C**), many animals treated with *swsn-4(RNAi)*
443 had single SMs that failed to divide and a mean DHB C/N ratio indicative of a long pause
444 or arrest in S phase (36) (Avg. C/N ratio = 0.803; n=20 SMs; **Fig S6 C**). Together, these
445 results suggested that the strength of our enhanced *swsn-4(RNAi)* targeting vector is
446 sufficient to recapitulate the *swsn-4* null condition in the SM lineage, as we detected both
447 the hypoproliferative phenotype and S-phase arrest that was observed using a lineage-
448 restricted catalytically inactive SWI/SNF ATPase (35).
449

450 **The BAF assembly contributes to AC invasion via regulation of G_0 cell cycle arrest**

451 Having established that strong depletion of the SWI/SNF complex results in a fully
452 penetrant defect in AC invasion with a high percentage of individual animals possessing
453 multiple non-invasive ACs (**Fig 3**), we next investigated whether the extra ACs observed
454 were the consequence of inappropriate AC proliferation (22,68). To determine whether
455 the SWI/SNF complex is required for G_0/G_1 cell cycle arrest in the AC, we quantified CDK
456 activity in the AC using a ubiquitously expressed *rps-27p::*DHB::GFP transgene paired
457 with AC (*cdh-3p::mCherry::moeABD*) and BM (*laminin::GFP*) reporters in live animals
458 following RNAi-mediated knockdown of SWI/SNF core (*swsn-4*), BAF (*swsn-8*), and
459 PBAF (*pbrm-1*) subunits (**Fig 4**). In wild-type invasive ACs, we observed strong nuclear

460 localization of the CDK sensor and quantified a cytoplasmic/nuclear (C/N) ratio indicative
461 of G_0/G_1 arrest (mean C/N ratio: 0.226+/-0.075, n=67 animals) (**Fig 4 A, F**). In order to
462 distinguish whether the wild-type AC C/N ratio is actually indicative of G_0 rather than G_1
463 arrest, we quantified the CDK activity in the neighboring uterine Pi cells at the P6.p 8 cell
464 1° VPC stage following their terminal division to establish a G_0 reference point (71,72)
465 (mean C/N ratio: 0.206+/-0.078, n=30 animals) (**Fig 4 E-F**). We found no significant
466 difference between the CDK activity of terminal Pi cells and wild-type invading ACs,
467 suggesting that the wild-type AC exists in a CDK^{low} G_0, pro-invasive state (**Fig 4 A, E-F**).
468 In animals treated with *pbrm-1(RNAi)*, the CDK sensor also localized principally in the
469 nucleus of ACs that failed to invade (mean C/N ratio: 0.157+/-0.063, n=41 animals) and
470 only a single non-invasive AC was observed per animal (**Fig 4 D, F**). In contrast, following
471 treatment with *swsn-8*(*RNAi*) the majority of ACs that failed to invade the BM were
472 in the G_1/S phases of the cell cycle (mean C/N ratio: 0.636+/-0.204, n=21 animals) (**Fig**
473 **4 C, F**). Finally, like the *swsn-8(RNAi)* condition, loss of expression of the core ATPase
474 of the SWI/SNF complex through treatment with *swsn-4*(*RNAi*) resulted in a broad range
475 of C/N ratios (C/N ratio min: 0.240, C/N ratio max: 1.140, mean C/N ratio: 0.566+/-0.205;
476 n=40 animals) in animals with single or multiple non-invasive ACs (**Fig 4 B, F**).
477 Interestingly, the *swsn-4(RNAi)* treatment resulted in a higher proportion of non-invasive
478 G_0 phase (C/N ratio < 0.3) ACs (14%, n=48 cells) than were present in the *swsn-8(RNAi)*
479 treated population (8%, n=25) (**Fig 4 B, E**). This finding reemphasizes the dependence
480 of both SWI/SNF BAF and PBAF assemblies on the core ATPase of the complex, as the
481 distribution of cell cycle states in ACs following *swsn-4(RNAi)* treatment represents both

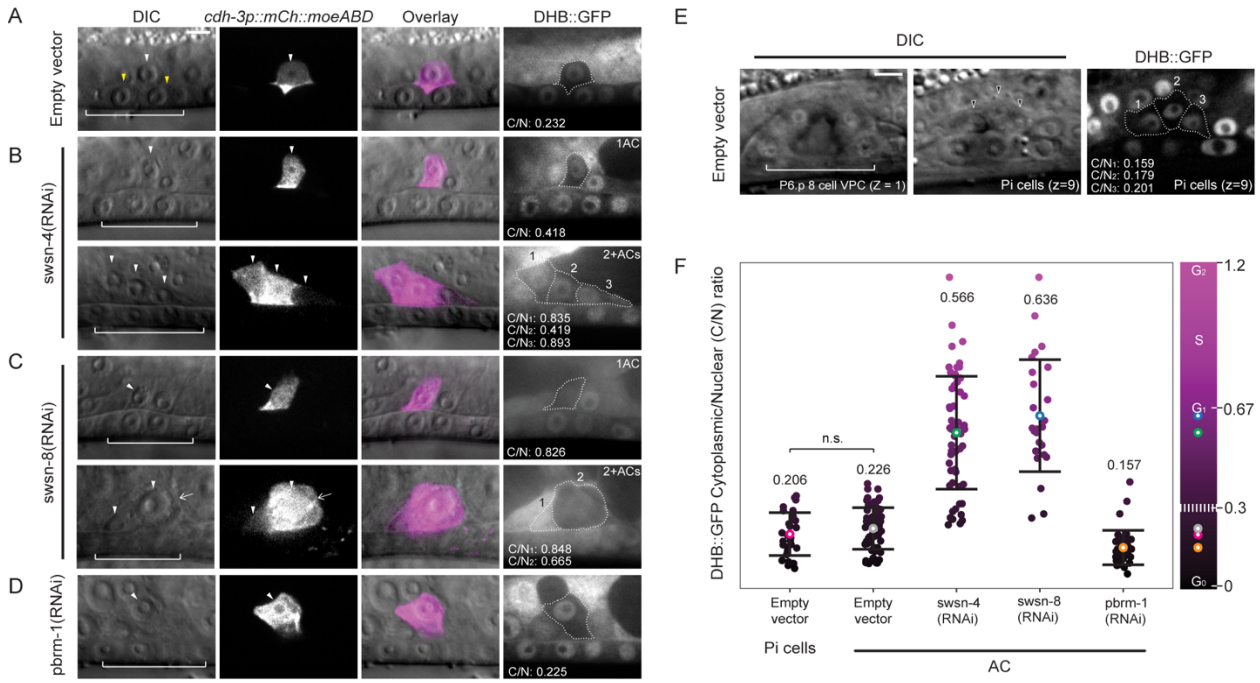

Figure 4. CDK sensor reveals SWI/SNF contribution to G_0 arrest in the AC. Micrographs depicting DIC (left), AC (*cdh-3p::mCherry::moeABD*, center-left), DIC overlay (center-right), and DHB-based CDK activity sensor (right) in empty vector **(A)** and following treatment with SWI/SNF RNAi targeting subunits of the core **(***swsn-4***, B)**, BAF **(***swsn-8***, C)** and PBAF **(***pbrm-1*, **D)** assemblies. White arrowheads indicate AC(s), yellow arrowheads indicate boundaries of breach in BM, and white brackets indicate 1° VPCs. In cases where treatment resulted in multiple cells expressing the AC reporter in the same animal, representative images of both single (1AC) and mitotic (2+ACs) phenotypes are given, and each AC is indicated with a single white arrowhead. Quantification of the cytoplasmic:nuclear (C/N) ratio of DHB::GFP in ACs (white dotted outline) is listed in the bottom left of each panel. Mitotic ACs are numbered, and C/N ratios are provided for each **(B-C)**. White arrowheads indicate AC(s), yellow arrowheads indicate boundaries of breach in BM, and white brackets indicate 1° VPCs. White arrow in C indicates an AC that is out of the focal plane. **(E)** Representative single z-plane micrographs of the vulva at the P6.p 8 cell stage (left, z=1) and the terminal Pi cells (middle, z=9) in DIC, and DHB-based CDK activity sensor in Pi cells (right). Quantification of the C/N ratio of DHB::GFP in three of four Pi cells (white dotted outline) that are in the plane of the image is listed in the bottom left. **(F)** Quantification of C/N DHB::GFP ratios for wild-type terminally divided Pi cells and all ACs in empty vector control and each RNAi treatment (n≥30 animals per treatment). Statistical comparison was made between the mean C/N ratio of ACs in control (empty vector) compared to control (empty vector) Pi cells using Student's *t*-test (n≥30 for each stage and subunit; p values are displayed above compared groups). Mean C/N ratio is represented by colored open circles and correspond to numbers above the data. Gradient scale depicts cell cycle state as determined by quantification of each Pi cell or AC in all treatments (n≥30 animals per treatment), with dark/black depicting G_0 and lighter/magenta depicting G_2 cell cycle states. Dashed white line on gradient scale bar (right) corresponds to boundaries between G_0 and G_1 phases. Colored open circles on the gradient scale correspond to the mean C/N ratio in each of the same color. n.s. not significant.

482 the cell cycle-dependent and cell cycle-independent phenotypes seen in ACs deficient in

483 the *swsn-8* and *pbrm-1* subunits, respectively

484

485 **Forced G_0 arrest through ectopic CKI-1 rescues invasive potential in BAF-deficient**
486 **but not PBAF-deficient ACs**

487 We have previously proposed and characterized a dichotomy that exists between
488 invasion and proliferation in the AC (22,24). As evidence of this, loss of two of the three
489 TFs that function in a cell cycle-dependent manner to maintain the AC in a cell cycle-
490 arrested state (*nhr-67*/Tlx and *hlh-2*/Daughterless) can be rescued through induced
491 expression of a cyclin dependent kinase inhibitor, *cki-1* (p21/p27) (22). These results
492 suggest that, at least in some cases, TF activity can be bypassed completely to promote
493 AC invasion by maintaining G_0 arrest through direct cell cycle manipulation. To determine
494 the extent to which the BAF assembly contributes to AC invasion through regulation of
495 cell cycle arrest, we used a heat-shock inducible transgene to ectopically express CKI-
496 1::mTagBFP2 in SWI/SNF-deficient ACs (**Fig 5**). Since the heat shock inducible
497 transgene is ubiquitous and expresses variably between different animals and different
498 tissues within an individual animal, we limited our analysis to animals with ACs with
499 obvious mTagBFP2 fluorescence expression. While forced arrest in G_0 was insufficient to
500 significantly rescue AC invasion in animals treated with *swsn-4(RNAi)* (**Fig 5 B, B', E**) or
501 *pbrm-1(RNAi)* (**Fig 5 D, D', E**), ectopic *cki-1* (CKI-1::mTagBFP2) expression in the AC
502 significantly rescued cellular invasion in animals treated with *swsn-8(RNAi)* (**Fig 5 C, C',**
503 **E**). Strikingly, in 85.7% (6/7) of cases where ACs had proliferated prior to ectopic CKI-1
504 expression, forced G_0 arrest led to multiple ACs breaching the BM (**Fig 5 F**), a phenotype
505 we have reported previously using CKI-1 overexpression paired with loss of NHR-67. This
506 demonstrated that mitotic ACs maintain the capacity to invade if they are re-arrested into

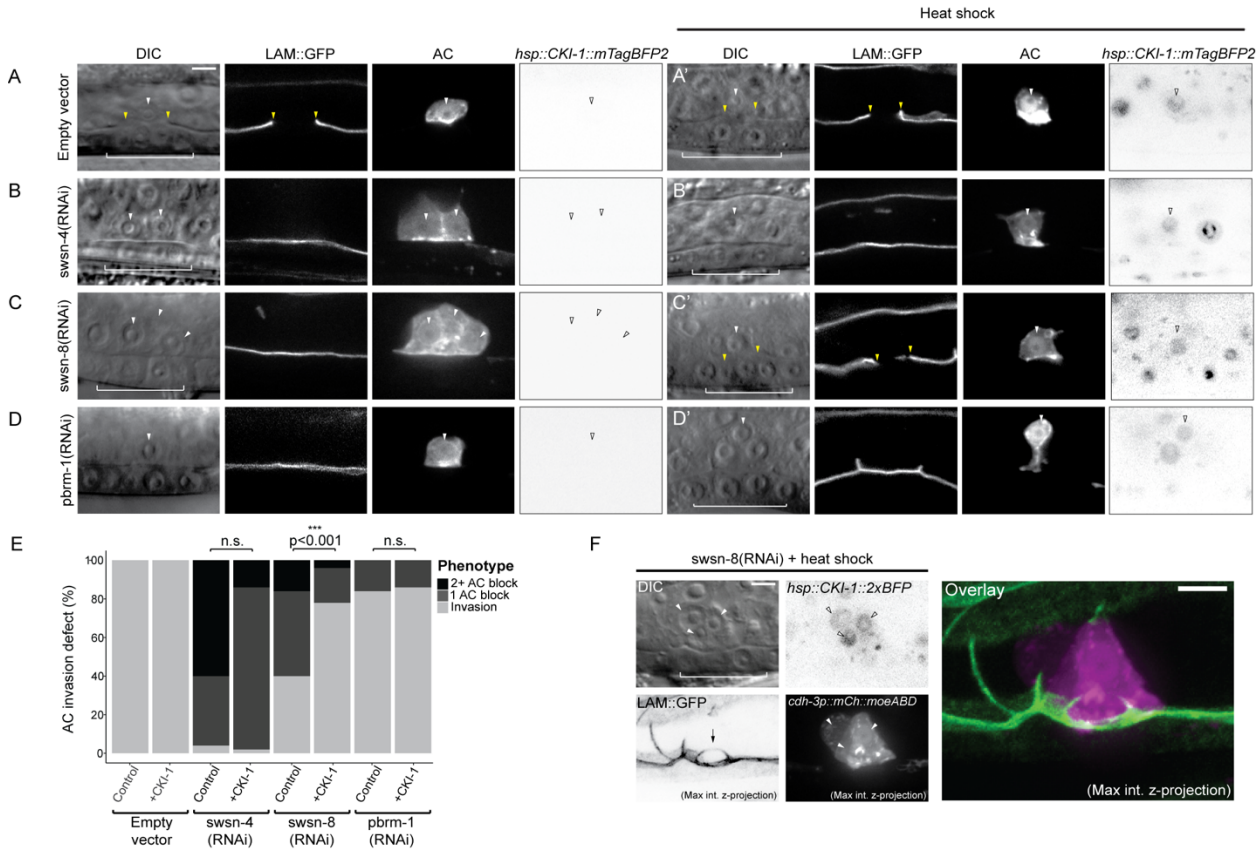

Figure 5. BAF depletion is rescued by G_0 arrest. Representative micrographs depicting DIC (left), BM (*laminin::GFP*, center-left), AC (*cdh-3p::mCherry::moeABD,* center-right), and CKI-1 (*hsp::CKI-1::mTagBFP2*) expression in empty vector control **(A-A')** and treatment with SWI/SNF RNAi under standard conditions **(A-D)** and following heat shock induction of CKI-1 **(A'-D')**. CKI-1 images have been inverted for ease of visualization. White arrowheads indicate AC(s), yellow arrowheads indicate boundaries of breach in BM, and white brackets indicate 1° VPCs. **(E)** Stacked bar chart showing percentage of AC invasion defects corresponding to each RNAi treatment under standard growth conditions (control) and following heat shock induction of CKI-1 (+CKI-1), binned by AC phenotype (n≥30 animals per condition; Fisher's exact test compared CKI-1(+) animals with control, non-heat shocked animals; p value is displayed above compared groups). n.s. not significant. **(F)** Representative micrographs of invasive group of *swsn-8* deficient ACs following induction of G_0/G_1 arrest. DIC (top-left), BM (bottom-left), CKI-1 expression (top-right), AC reporter (bottom-right). Max intensity z-projection of AC and BM reporter channels (bottom). Large breach in BM is indicated by black arrow.

507 a G_0 state (24). To corroborate our CKI-1 heat shock data, we used an AC-specific CKI-
508 1 transgene (*cdh-3p::CKI-1::GFP*) to induce G_0 cell cycle arrest in *swsn-4-* and *swsn-8-*
509 depleted ACs (**Fig S6**). Similar to the heat shock results, lineage-restricted expression of
510 CKI-1::GFP failed to rescue invasion in animals deficient in *swsn-4* (**Fig S7 A-B**).
511 However, transgenic *cdh-3p::CKI-1::GFP* animals treated with *swsn-8(RNAi),* had

512 invasion defects significantly lower than control animals treated with *swsn-8(RNAi)* which
513 lacked the G_0 rescue transgene (**Fig S7 B**). Altogether, these data corroborate our DHB-
514 based CDK sensor data (**Fig 4**), suggesting that the SWI/SNF assemblies differentially
515 contribute to AC invasion with BAF specifically required for G_0 cell cycle arrest.
516

517 **SWI/SNF chromatin remodeling promotes the invasive GRN in the AC**

518 Previous work has demonstrated that the gene regulatory network (GRN) that
519 promotes AC invasion consists of both cell cycle-dependent and cell cycle-independent
520 TF subcircuits (22,68) (**Fig 1 B**). In the cell cycle-dependent subcircuit of the TF-GRN,
521 *egl-43* (EVI1/MEL), *hlh-2* (E/Daughterless), and *nhr-67* (TLX/Tailless) cooperate in a type
522 1 coherent feed-forward loop that is reinforced via positive feedback to retain the AC in a
523 post-mitotic, invasive state (22,68). The cell cycle-independent subcircuit of the AC TF-
524 GRN is governed by the *fos-1* (FOS) TF with feedback from both *egl-43* and *hlh-2* (22).
525 Since transcriptional knockdown of SWI/SNF ATPase results in both single and mitotic
526 non-invasive AC phenotypes, we treated endogenously GFP-labeled strains for each TF
527 in the GRN with *swsn-4(RNAi)* to determine whether SWI/SNF chromatin remodeling
528 contributes to the regulation of either or both AC GRN subcircuits (**Fig 6**). In the cell cycle-
529 dependent subcircuit, knockdown of the SWI/SNF ATPase resulted in significant loss of
530 protein expression of EGL-43::GFP and NHR-67::GFP in the AC (39% and 26% GFP
531 depletion, respectively; n≥41 animals; **Fig 6 A,C,E**). No significant difference was
532 detected in the mean fluorescence expression of GFP::HLH-2 fusion protein in the AC
533 upon knockdown of *swsn-4,* however the range of expression was broad following *swsn-*
534 *4(RNAi)* treatment (~2% GFP increase; n≥50 animals; **Fig 6 B, E**). In the cell cycle-

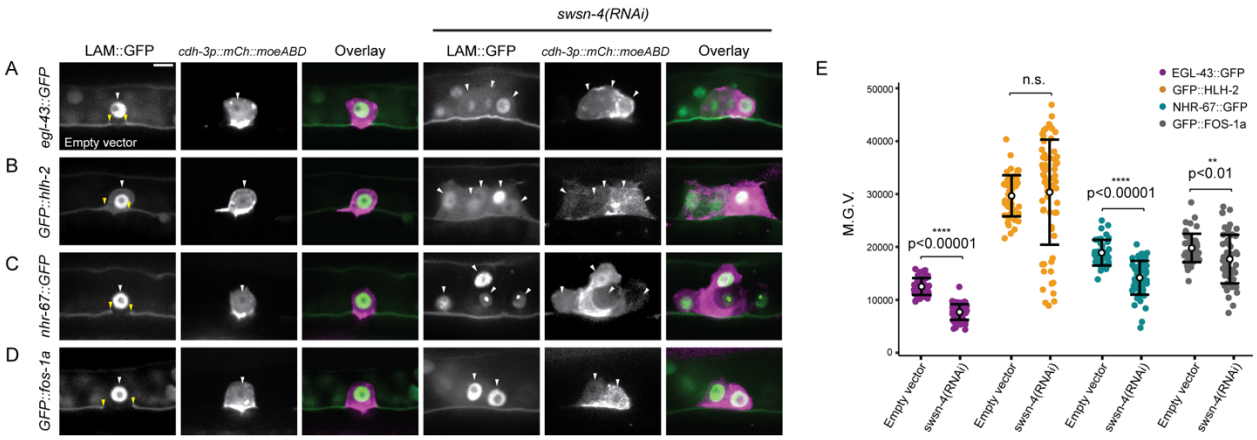

Figure 6. SWI/SNF regulates endogenously tagged TFs in the AC invasion GRN. Fluorescent micrographs depicting BM (*lam::GFP*) and AC (*cdh-3p::mCherry::moeABD*) expression of endogenously tagged TFs of the cell cycle-dependent subcircuit (*egl-43::GFP::egl-43* **(A),** *GFP::hlh-2* **(B),** and *nhr-67::GFP* **(C)**) and cell cycle-independent subcircuit (*GFP::fos-1a* **(D)**) of the AC GRN in animals treated with empty vector control (left) or *swsn-4(RNAi)* (right). White arrowheads indicate AC(s), yellow arrowheads indicate boundaries of breach in BM. **(E)** Quantification of fluorescent expression of each TF::GFP in ACs of control animals and animals treated with *swsn-4(RNAi)*. Statistical comparisons were made between the expression of each TF subunit in the AC in control and RNAi-treated animals using Student's *t*-test (n≥30 for each condition; p values are displayed above black brackets). n.s. not significant.

535 independent subcircuit, loss of the SWI/SNF complex following treatment of *fos-1::GFP*
536 animals with *swsn-4(RNAi)* resulted in a more moderate depletion of expression in the
537 AC (11% GFP depletion; n≥50 animals; **Fig 6 D**). These results suggest that the SWI/SNF
538 complex broadly remodels chromatin to promote both subcircuits of the pro-invasive AC
539 GRN, though we are unable to determine whether the complex does so directly in
540 regulatory regions of the lineage-specific pro-invasive TFs or in regulatory regions of
541 genes that contribute to the regulation of the AC GRN.
542

543 **The PBAF assembly regulates AC contact with underlying BM**

544 Previous investigations into SWI/SNF have demonstrated divergent roles for the PBAF
545 assembly in cell cycle regulation. In yeast, Remodeling the Structure of Chromatin (RSC),
546 the homologous complex to PBAF, is required for progression through mitosis (73,74). In

547 *Drosophila,* the homologous complex PBAP does not appear to be required for mitotic
548 progression; rather, cycling and G_2/M transition is solely regulated by the BAF/BAP
549 assembly (51). In the *C. elegans* M lineage, RNAi-mediated loss of BAF subunits results
550 in hyperproliferation of the developing tissue, whereas knockdown of PBAF subunits has
551 little effect on cell cycle control (35). Similarly, in this study, RNAi-mediated loss of PBAF
552 subunits *pbrm-1*, *swsn-7*, or *swsn-9* resulted exclusively in single non-invasive cells
553 expressing the AC reporter. However, given that the enhanced *pbrm-1(RNAi)* resulted in
554 much weaker endogenous protein knockdown than the enhanced RNAis targeting either
555 the SWI/SNF ATPase (*swsn-4*) or BAF assembly subunit (*swsn-8*) in the AC (**Fig S4**),
556 and the dose-dependent phenotype following loss of the core ATPase (**Fig 3**), it is
557 possible that we failed to observe the mitotic non-invasive AC phenotype due to
558 insufficient PBAF subunit knockdown. To address this, we next asked whether *strong*
559 loss of PBAF subunit expression contributes to the mitotic non-invasive AC phenotype.
560 To accomplish this, we used an auxin inducible degron (AID)-RNAi combination
561 knockdown strategy (75,76). We generated a strain with *pbrm-1* endogenously labeled
562 with mNeonGreen and an auxin inducible degron (AID) (*pbrm-1::mNG::AID*) in a genetic
563 background containing AC (*cdh-3p::mCherry::moeABD*) and BM (*laminin::GFP*)
564 reporters. We then quantified fluorescence expression in the AC in this strain. When
565 grown under standard conditions, 6.45% of the ACs had not invaded the BM by the P6.p
566 4 cell stage, suggesting a partial loss of function of *pbrm-1* (n=30; **Fig 7 A, E-F**). This
567 partial loss of function phenotype is likely due to the insertion of the mNG::AID tag into
568 the genomic locus, causing a putative hypomorphic allele. Next, we introduced a
569 ubiquitous, mRuby-labeled TIR1 transgene (*eft-3p::TIR1::mRuby*) into the animals and

570 assessed AC invasion under standard conditions (aux(-)) or in the presence of the auxin
571 hormone (aux(+); **Fig 7 B**). We observed no statistically significant difference in the
572 fluorescence expression of PBRM-1::mNG::AID protein in the AC, nor did we observe
573 any differences in AC invasion defects between the strains with and without the TIR1
574 transgene when grown on aux(-) media (TIR1+: 3% depletion, 16.67% invasion defect;
575 n=30; **Fig 7 E-F**). However, in both conditions, some ACs that invaded seemed to do so
576 only partially, as most of the ventral epidermal BM remained intact beneath ACs (**Fig 7**
577 **B**, black arrowhead). In the aux(+) condition, there was a significant reduction in PBRM-
578 1::mNG::AID protein level in the AC of animals containing the TIR1 transgene relative to
579 the same strain grown in the aux(-) condition or the strain without the TIR1 transgene
580 (49% and 51% depletion, respectively; n=30; **Fig 7 E**); however, there was no significant
581 difference in the penetrance of AC invasion defects (16.67% invasion defect; n=30; **Fig 7**
582 **F**). Like our previous results with *pbrm-1(RNAi)* treated animals, we observed no extra
583 cells expressing the AC reporter following loss of expression of PBAF in the AC using the
584 AID system.

585 Next, we treated *pbrm-1::mNG::AID* animals containing ubiquitous TIR1 with
586 *pbrm-1(RNAi)* in both aux(-) and aux(+) conditions. As expected, treatment of the *pbrm-*
587 *1::mNG::AID* strain with *pbrm-1(RNAi)* resulted in very low expression of the subunit in
588 the AC even in the absence of auxin and there was no significant difference in expression
589 between the Aux(-) and Aux(+) conditions (**Fig 7 C,F**). Interestingly, there was also no
590 significant difference in the penetrance of AC invasion defects between the *pbrm-*
591 *1::mNG::AID* strain treated with control compared to the strain treated with *pbrm-1(RNAi)*
592 in the presence of auxin (**Fig 7 G**). Since the combination treatment of a hypomorphic

593

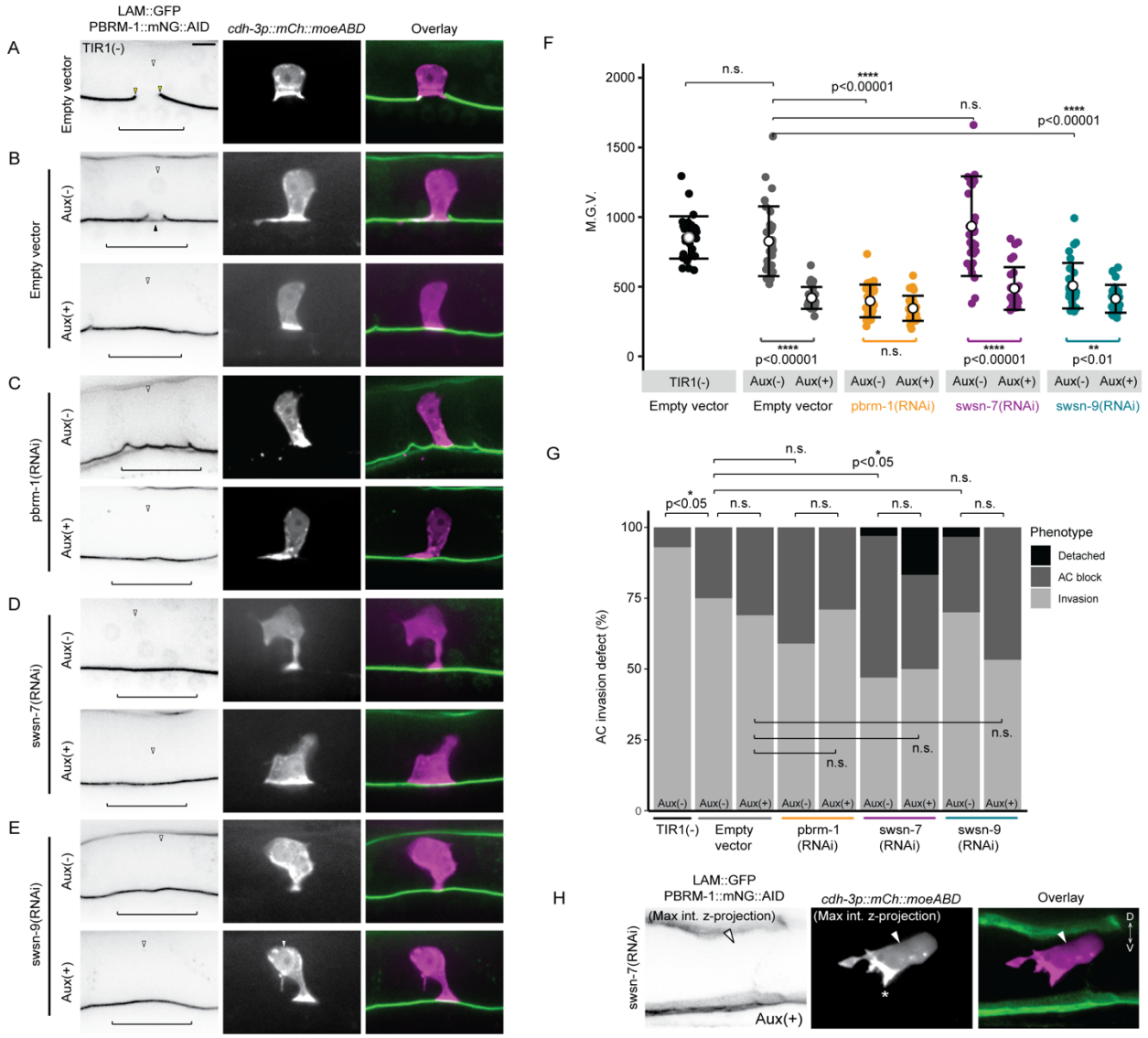

Figure 7. PBAF promotes AC contact to the BM. Representative micrographs of BM (*lam::GFP*) and endogenous *pbrm-1::mNG::AID* (left), AC (*cdh-3p::mCherry::moeABD*, center), and fluorescent overlays (right) of animals lacking **(A)** or possessing **(B-E)** ubiquitous TIR1 expression treated with empty vector control **(B)** or RNAi targeting PBAF subunits in the absence Aux(-) (top) or presence Aux(+) (bottom) of media containing the auxin hormone **(C-E).** PBRM-1::mNG::AID images have been inverted for ease of visualization. **(F)** Quantification of fluorescence expression (M.G.V) of PBRM-1::mNG::AID in ACs of animals in each condition (N≥30 animals in each treatment; p values for Fisher's exact test comparing strains containing TIR1 to the TIR1(-) strain, and comparing strains containing TIR1 in the Aux(-) to the Aux(+) condition, are displayed above compared groups). **(G)** Stacked bar chart showing percentage of AC invasion defects corresponding to each treatment, binned by AC phenotype (N≥30 animals per condition; Fisher's exact test compared penetrance of AC invasion defects between indicated conditions). Black brackets indicate statistical significance between invasion total in each condition compared to invasion defect total. **(H)** Max intensity z-projection of AC and BM reporter channels depicting a detached AC phenotype in *swsn-7*-deficient ACs in the Aux(+) condition. BM (left), AC (center), fluorescence overlay (right). Asterisk indicates polarized F-actin driven protrusion extending ventrally.

594 *pbrm-1* allele, Auxin-AID-mediated depletion of endogenous PBRM-1::mNG::AID, and
595 *pbrm-1(RNAi)* does not result in a significant increase in AC invasion defects or non-
596 invasive mitotic ACs, these results suggest that, unlike the dose-dependent contribution
597 to invasion of *swsn-4*, the *pbrm-1* strong knockdown or null phenotype may be only
598 partial/incomplete loss of AC invasion.

599 Since the PBAF assembly in *C. elegans* consists of several subunits, *pbrm-1*
600 (PBRM1), *swsn-7* (ARID2), and *swsn-9* (BRD7/BRD9), we next investigated whether
601 combinatorial knockdown of PBAF subunits would enhance the penetrance of AC
602 invasion defects or result in the mitotic non-invasive AC phenotype. In the absence of
603 auxin, there was no significant difference in PBRM-1::mNG::AID expression in the AC of
604 animals treated with *swsn-7(RNAi)* compared to animals treated with empty vector control
605 (n=30; **Fig 7 E**), however there was a significant increase in loss of AC invasion (50%
606 invasion defect; n=30; **Fig 7 F**). Strikingly, in one case, the AC was completely detached
607 from the BM, as we detected no AC membrane protrusions (*cdh-3p::mCherry::moeABD*)
608 in contact with the ventral surface of the gonad (**Fig 7 F**). Animals treated with *swsn-*
609 *7(RNAi)* and aux(+) had significantly lower expression of PBRM-1::mNG::AID in the AC
610 when compared to animals treated with *swsn-7(RNAi)* in the aux(-) condition (49%
611 depletion; n=30; **Fig 7 E**). While no significant difference was seen in loss of AC invasion
612 in aux(+) (48.39% AC invasion defect), 16% (5/31) of animals in this treatment had ACs
613 entirely detached from the ventral BM (n=31; **Fig 7 F-G**). In contrast to treatment with
614 *swsn-7(RNAi)*, in the *swsn-9(RNAi)* aux(-) condition, PBRM-1::mNG::AID expression in
615 ACs was significantly lower than that in the ACs of animals treated with empty vector
616 control aux(-) (39% depletion; n=30; **Fig 7 E**). It is unclear why transcriptional knockdown

617 of *swsn-9* specifically results in a decrease in PBRM-1 protein expression in the AC and
618 we theorize this may be the result of a potential stabilizing interaction between the SWSN-
619 9 and PBRM-1 proteins. We did detect a significant decrease in expression of PBRM-
620 1::mN G::AID in ACs in *swsn-9(RNAi)* aux(+) compared to the *swsn-9(RNAi)* aux(-)
621 condition (19% depletion; n=30; **Fig 7 E**), however, we saw no statistically significant
622 difference in penetrance of AC invasion defects between the two conditions (30% vs.
623 43%; n=30; **Fig 7 F**). We also noted one animal with a detached AC in the *swsn-9(RNAi)*
624 aux (-) condition and zero in the aux(+) condition (**Fig 7 F**). Importantly, we only observed
625 one AC per animal across all combinatorial treatments, supporting the hypothesis that the
626 PBAF assembly does not contribute to G_0 cell cycle arrest in the AC.

627 Detached ACs in both the *swsn-7(RNAi)* and *swsn-9(RNAi)* AID combination
628 knockdown conditions suggest that the PBAF assembly regulates AC contact with the
629 ventral epidermal BM. A previous study has shown that AC attachment is regulated by
630 the *fos-1/egl-43* cell cycle-independent subcircuit of the AC GRN via regulation of
631 lamellipodin/*mig-10b* and non-autonomously via netrin/*unc-6* signaling (77). ACs deficient
632 in components of this pathway are attached to the ventral epidermal BM when specified
633 and gradually lose contact over time, with peak loss of contact occurring at the time of AC
634 invasion at the P6.p 4-cell stage (77). In order to determine whether the PBAF assembly
635 remodels chromatin to promote activation of this subcircuit of the AC GRN, we treated
636 endogenously tagged *fos-1::GFP* (22) animals with *pbrm-1(RNAi)* and quantified
637 fluorescence expression in ACs that displayed invasion defects (**Fig S8 A-B**). Animals
638 treated with *pbrm-1(RNAi)* had a modest but statistically significant loss of FOS-1::GFP
639 protein levels in non-invasive ACs (34% depletion; n=20; **Fig S8 B**), suggesting that the

640 PBAF assembly partially regulates the *fos*-dependent pathway that mediates attachment
641 to the underlying BM.

642 Since depletion of the PBAF assembly resulted in moderate loss of FOS-1::GFP
643 in the AC, we next examined functional interactions between FOS-1 and PBRM-1. Given
644 that the PBRM-1::mNG::AID allele was slightly hypomorphic, with ~17% invasion defects
645 in backgrounds with TIR1, we used the strain containing TIR1 as a sensitized
646 background. We found that even without the addition of auxin, co-depletion with *fos-*
647 *1(RNAi)* resulted in almost complete loss of AC invasion (96.77% invasion defect; n=31;
648 **Fig S8 C-D**). Finally, we examined whether RNAi-mediated depletion of *pbrm-1* is
649 synergistic with loss of downstream targets of FOS-1, the matrix metalloproteinases
650 (MMPs). Previously, it has been shown that animals harboring null mutations for five of
651 the six MMPs encoded in the *C. elegans* genome (*zmp-1,-3,-4,-5* and *-6*), show delayed
652 AC invasion (21). RNAi depletion of *pbrm-1* in quintuple MMP mutants significantly and
653 synergistically enhanced late invasion defects (scored at the P6.p 8-cell stage) in this
654 background (24.24% invasion defect; n=33; **Fig S8 E-F**) as compared to loss of either
655 *pbrm-1* (3.8%; n=52) or MMPs (0%; n=35) alone. Together, these results suggest that the
656 PBAF assembly functions synergistically with FOS-1 to regulate AC invasion.

657

658 **DISCUSSION**

659 **A tissue-specific CRF RNAi screen identified genes critical for cellular invasion**

660 Previous work in the *C. elegans* AC and in cancer cell invasion has emphasized
661 the necessity for dynamic chromatin states and chromatin regulating factors in the
662 promotion of cellular invasion (24,79–83). In this study, we used the *Caenorhabditis*

663 *elegans* AC invasion model as a single cell, *in vivo* system to identify a suite of CRFs that
664 contribute to the process of cellular invasion. We performed a tissue-specific RNAi
665 feeding screen to assess 269 genes implicated in chromatin binding, chromatin
666 remodeling complexes, or histone modification. We do not claim that genes that we failed
667 to identify as regulators of cellular invasion in the screen are unimportant for the process;
668 however, RNAi-mediated loss of the majority of CRF genes in the screen did result in
669 some penetrance of AC invasion defects (**Table S1**). This finding was expected, as many
670 of the genes we screened are global regulators of the genome and broadly contribute to
671 various cell biological processes. We extracted a list of the most penetrant regulators of
672 cell invasion from the broader list (**Table S2**). Many genes and gene classes that we
673 recovered as significant regulators of AC invasion are homologous to human genes that
674 have been previously studied in the context of cellular invasion and tumorigenesis
675 including *cec-6*/CBX1/CBX8 (82,84), *cfi-1*/ARID3A/ARID3C (85), *psr-1*/JMJD6 (86), *skp-*
676 *1*/SNW1 (87), and several TAFs (*taf*-1/TAF1/TAF1L, taf-*5*/TAF5/TAF5L, *taf-*
677 *7.1*/TAF7/TAF7L) (88–90). Additionally, we recovered nematode-specific genes including
678 *nra-3, and cec-2,* and genes whose human homologs have not been previously studied
679 in the context of cellular invasion to our knowledge, such as *cec-3* (homologous human
680 protein is uncharacterized) and *gna-2*/GNPNAT. Since the majority of the CRF genes we
681 identified as significant regulators of AC invasion have been previously studied in the
682 context of invasion in human development and cancer metastasis, these results
683 demonstrate the utility of the *C. elegans* AC invasion system as a genetically and optically
684 tractable *in vivo* environment to corroborate and characterize previously identified CRFs
685 that promote cellular invasion in human diseases such as rheumatoid arthritis and cancer.

686 Future studies should continue to characterize the relationship between CRFs identified
687 here and cellular invasion.
688

689 **The dose of SWI/SNF ATPase dictates the penetrance of defects in AC invasion**

690 For the majority of this study, we focused on characterizing the contribution of the
691 SWI/SNF ATP-dependent chromatin remodeling complex to cellular invasion as it was
692 highly represented among our list of significant regulators of AC invasion (**Table S2**) and
693 has been extensively studied in the context of both cellular invasion and cell cycle control
694 across a variety of animal models and in human cancers (31,35,40,42,48,56,59,83,91–
695 96). Prior whole-exome studies have determined that over 20% of human tumors harbor
696 mutations in one or more subunits of the SWI/SNF complex (32,48,98). Among the most
697 frequently mutated subunits of the chromatin remodeling complex throughout SWI/SNF-
698 deficient cancers is the core ATPase subunit BRG1/SMARCA4 (48,99) and the mutually
699 exclusive ATPase paralog to BRG (32,81,98,100).

700 Due to the high degree of structural similarity between BRG and BRM, mutation or
701 epigenetic silencing of either ATPase can be compensated by expression of the other.
702 Previous investigation has determined BRM to be an effective synthetic lethal target in
703 BRG1-deficient cancer, and vice-versa (101,102). Despite the compensatory nature of
704 BRG1/BRM in many tumorigenic contexts, concomitant loss of expression of the
705 ATPases has been described in metastatic murine models and patient-derived non-small-
706 cell lung cancer (NSCLC) cell lines and is associated with poor patient survival
707 (91,103,104). In *C elegans*, the sole SWI/SNF ATPase, *swsn-4,* has a high degree of
708 homology to both mammalian BRG1 and BRM, providing a unique opportunity to

709 accessibly model the connection between the dual loss of BRG1/BRM associated with
710 poor prognostic outcomes in NSCLC and cellular invasion in the AC. Additionally, a recent
711 study demonstrated a phenotypic dosage-sensitivity following loss of SWI/SNF
712 expression in relation to terminal differentiation of *C. elegans* muscle and vulval tissues
713 (35), suggesting that the context- and dose-dependent relationship seen in mammalian
714 development and SWI/SNF-deficient cancers may represent a more general behavior of
715 the complex.

716 Here we used the *C. elegans* AC invasion system as a model to investigate
717 whether the dose-dependent relationship between the ATPase and differentiated
718 phenotype extends to cellular invasion. The first indication that the functional dose of
719 SWI/SNF may have an instructive role in AC invasion was the relative enhancement of
720 all endogenously tagged subunits of the complex in the AC relative to neighboring VU
721 and VPC tissues (**Fig S4**). While it is tempting to interpret the enhancement of SWI/SNF
722 subunit expression in the AC as evidence for the dependence of cellular invasion on
723 SWI/SNF activity, it is also possible that this difference in expression is a consequence
724 of terminal differentiation, since at the time of invasion, the AC is terminally differentiated
725 unlike the VU and VPC). Further investigation is required to determine whether
726 endogenously tagged SWI/SNF subunits are enhanced in the AC relative other terminally
727 differentiated cells.

728 Additionally, we find that some degree of SWI/SNF intra- and inter-complex
729 regulation exists in the AC at the time of invasion with both SWI/SNF assemblies
730 cooperating to activate expression of the ATPase (**Fig S5 B**). It is possible that this added
731 level of complex autoregulation contributes to an “optimal” dose of the ATPase in a cell-

732 and context-specific manner. It is important to note that the model proposed in Fig S5 F
733 is incomplete and is included to describe the translational consequence of individual
734 SWI/SNF subunits after transcriptional knockdown of other individual SWI/SNF subunits.
735 However, these data can be meaningfully used to inform interpretations of results for our
736 enhanced SWI/SNF RNAi experiments in the AC.

737 To directly correlate SWI/SNF dose and invasive phenotype in the AC, we used a
738 combination of an enhanced *swsn-4(RNAi)* vector with a tissue-specific antiGFP-
739 targeting nanobody construct. These combined technologies allowed us to titrate the dose
740 of ATPase in the AC at the time of invasion. By assessing AC invasion phenotypes at
741 wildtype levels of SWSN-4 and in moderate and severe ATPase knockdown conditions,
742 results indicate that cellular invasion and cell cycle control depends on the dose of
743 functional SWI/SNF present in the AC.

744 In addition to reflecting the dose-dependent nature of the SWI/SNF ATPase in
745 cancer, our data in the AC is consistent with work done in *C. elegans* early mesoblast
746 development where complete loss of the *swsn-4* ATPase using a catalytically dead
747 mutant and lineage-specific knockout strategy results in loss of cell cycle arrest (35).
748 Although we cannot be sure that combining *swsn-4(RNAi)* with an antiGFP-targeting
749 nanobody to deplete the SWI/SNF ATPase results in complete loss of protein expression,
750 we show that treatment with the improved *swsn-4(RNAi)* vector alone is sufficient to
751 phenocopy the null phenotype previously reported in late mesoblast (SM) development
752 (**Fig S6**). Additionally, enhancement of the AC mitotic phenotype statistically tracked with
753 a progressive step down in mean expression of the ATPase in the AC across our
754 experiments. Using endogenous fluorescent reporters for conserved pro-invasive genes,

755 we also provide evidence that the SWI/SNF complex is involved broadly with the
756 regulation of the cell cycle- dependent and -independent subcircuits of the AC GRN (**Fig**
757 **6**). Altogether, this data supports the hypothesis that SWI/SNF cell-autonomously
758 contributes to cell cycle control in a dose-dependent manner and provides the first line of
759 evidence to link SWI/SNF ATPase dosage to the dichotomy between invasion and
760 proliferation (**Fig 8**).
761

762 **The SWI/SNF BAF assembly promotes cellular invasion through induction of G_0**
763 **cell cycle arrest**

764 While previous work in our lab, based on localization of a DNA licensing factor,
765 CDT-1, has demonstrated indirectly that ACs must arrest in a G_0/G_1 cell cycle state
766 (22,24), we lacked a sensitive enough tool to distinguish between these two interphase
767 states. From our recent work utilizing a CDK sensor to examine the proliferation-
768 quiescence decision in *C. elegans*, we can distinguish between pre-terminal cells in the
769 somatic gonad in G_1 (mean C/N ratio: 0.67+/-0.10) as compared to terminally
770 differentiated G_0 uterine cells (mean C/N ratio: 0.30+/-0.11) (36). Here, we compare CDK
771 activity measurements in the ACs of control animals with that of the terminal Pi lineage to
772 provide the first quantitative demonstration that ACs arrest in a CDK^{low} G_0 state to invade
773 (**Fig 4 A, E, F**). Furthermore, by combining the CDK sensor with loss of SWI/SNF
774 subunits, our data indicate that the SWI/SNF BAF assembly is specifically responsible for
775 regulation of G_0 cell cycle arrest in the AC.
776
777

778

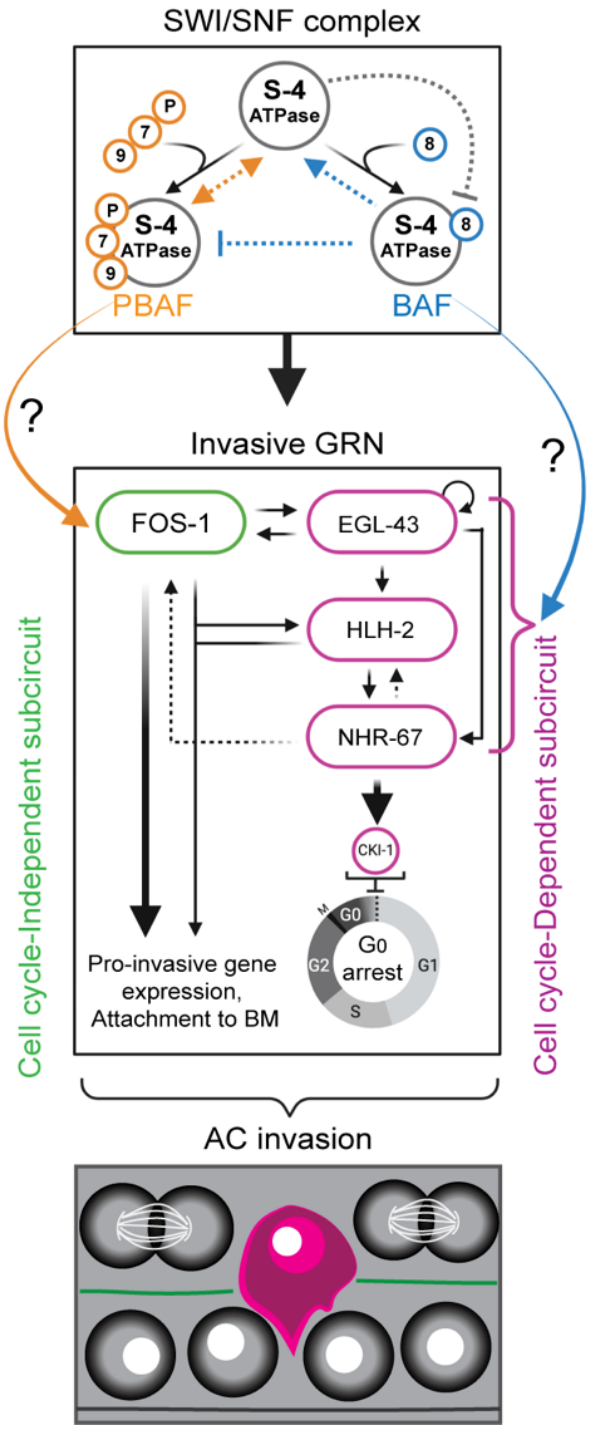

Figure 8. SWI/SNF complex promotes AC invasion. Schematic summary of the how the SWI/SNF ATPase (S-4*, swsn-4*), PBAF (orange – S-7, swsn-*7*; S-9, *swsn-9*; P, *pbrm-1*), and BAF (blue – S-8, *swsn-8*) assemblies contribute to AC invasion.

779 The SWI/SNF core complex is composed of an ATPase, core, and accessory
780 factors, which are thought to collectively provide a platform of common factors that is
781 bound by assembly-specific subunits in a mutually exclusive manner. In *C. elegans*, the
782 association of SWSN-8 (BAF250a/ BAF250b/ ARID1A/ ARID1B) with the common factors
783 forms the SWI/SNF BAF assembly. Since we identified representative subunits from the
784 core of the complex and both SWI/SNF BAF and PBAF assemblies in our CRF RNAi
785 screen, we took a cell biological and genetic approach to investigate the role of the each
786 SWI/SNF assembly in promoting cellular invasion. Here, using a DHB-based CDK sensor
787 (36,70), we show that loss of either core or BAF assembly subunits specifically results in
788 mitotic ACs that failed to invade the BM. Our cell cycle sensor data first establishes that
789 wild-type AC invades in a G_0 CDK^{low} state, and second, that a major contribution of the
790 BAF assembly to AC invasion is through maintenance of this G_0 arrest, as many ACs that
791 failed to invade the BM had increasing CDK activity, indicative of cells cycling in G_1, S or
792 G_2. Alternatively, 14% of ACs that failed to invade the BM following loss of *swsn-*
793 *4*/ATPase of the complex had CDK activity ratios indicative of G_0 cell cycle arrest,
794 suggesting a cell cycle-independent defect. In support of this, forced arrest of BAF-
795 deficient ACs in G_0 was sufficient to significantly rescue invasion, whereas CKI-1
796 induction failed to rescue invasion in ACs with RNAi-mediated loss of *swsn-4*/ATPase.
797 Altogether, our results indicate that the SWI/SNF complex contributes to AC invasion
798 through regulation of G_0 cell cycle arrest via the BAF assembly. Further investigation will
799 require biochemical techniques to identify cell cycle regulators and TF targets of the BAF
800 assembly to provide a mechanistic explanation for how exactly BAF regulates the
801 chromatin landscape to promote invasion (**Fig 8**, blue arrow). Targeted DNA adenine

802 methyltransferase identification (TaDa) is an attractive biochemical approach that may be
803 adaptable to the AC invasion system, as this approach has been characterized as an
804 effective, tissue-specific method to identify TF-target sequence interactions in the *C.*
805 *elegans* epidermis (106).
806

807 **The PBAF assembly regulates AC invasion and attachment to the BM**

808 Based on homology and phenotypic characterization in this study and previous
809 publications, the *C. elegans* PBAF assembly consists of the PBRM-1 (PBRM1/BAF180),
810 SWSN-7 (BAF200/ARID2), and SWSN-9 (BRD7/BRD9) in association with the SWI/SNF
811 common factors. Previous work in *C. elegans* has not revealed a connection between
812 the PBAF assembly and cell cycle arrest. Our initial experiments with improved RNAi
813 vectors targeting PBAF subunits resulted in a lower penetrance of AC invasion defects
814 relative to loss of core or BAF subunits. Additionally, our CDK sensor data suggested that
815 non-invasive ACs deficient in *pbrm-1* remain in a G_0 cell cycle state. Thus, our data shows
816 no PBAF contribution to cell cycle control in the AC. To confirm this, we used the auxin
817 inducible degron (AID) system to robustly deplete the PBAF assembly through combined
818 loss of endogenous PBRM-1::mNG::AID with RNAi-mediated knockdown of either of the
819 other two PBAF assembly subunits, *swsn-7* or *swsn-9*. This combination knockdown
820 strategy corroborated our previous results as we saw no significant penetrance of extra
821 ACs. Rather, here we associate a striking AC detachment phenotype with strong
822 combined knockdown of the PBAF assembly subunits. We also note aberrant BM
823 morphology in some ACs deficient in PBAF subunits, with only one of the two BMs
824 removed, suggesting that this assembly regulates attachment and extracellular matrix

825 (ECM) remodeling in wild-type ACs to promote invasion. We hypothesize that the PBAF
826 assembly is regulating ventral BM attachment and ECM remodeling potentially through
827 the regulation of HIM-4/Hemicentin, an extracellular immunoglobulin-like matrix protein
828 that functions in the AC to fuse the two BMs through the formation of a novel BM-BM
829 adhesion, the B-LINK (107). Finally, although RNAi-mediated transcriptional knockdown
830 of PBAF assembly subunits only partially depleted levels of FOS-1::GFP, a key TF
831 responsible for the expression of MMPs and other pro-invasive targets, we detected
832 significant enhancement of invasion defects when depleting *fos-1* in a putative
833 hypomorphic *pbrm-1* background. Reciprocally, depletion of *pbrm-1* enhanced the
834 invasion defect of a quintuple MMP mutant. Since we noted multiple instances of AC-BM
835 detachment following PBAF assembly subunit depletion, we propose that PBAF functions
836 in part with FOS-1 to facilitating activating chromatin states at the regulatory regions of
837 pro-invasive genes required for BM attachment. Future studies should include an
838 investigation of PBAF assembly interactions with other FOS effectors and interactors at
839 the transcriptional level. Additionally, given the broad genomic regulation exhibited by
840 chromatin remodelers, biochemical techniques such as chromatin immunoprecipitation
841 (ChIP) and single cell RNA sequencing will be crucial going forward to generate a
842 comprehensive roster of direct and indirect targets of each SWI/SNF assembly in the AC.
843 Collectively, these results reveal a distinct contribution for each SWI/SNF assembly to the
844 process of cellular invasion at the phenotypic level and reiterate the dependence of each
845 assembly on the functional dose of ATPase in a cell.
846
847

ACKNOWLEDGEMENTS

We are thankful to David Gray, Ed Luk, Laura Mathies, Benjamin Martin, Robert Morabito, Valerie Reinke, Courtney Tello, and Gerald Thomsen for advice and comments on this manuscript. We would also like to thank Thom Geer of Nobska Imaging for advice and 'scientific enabling'. Some *C. elegans* strains were provided by the CGC, which is funded by NIH Office of Research Infrastructure Programs (P40 OD010440).

AUTHOR CONTRIBUTIONS

J.J.S. and D.Q.M. designed the experiments. J.J.S., Y.X., M.A.Q.M., and T.N.M.-K. performed the experiments. J.J.S., A.Q.K., and M.C. organized the CRF RNAi screen. J.J.S., M.C., N.P., and Y.X. performed the RNAi screen. J.J.S., A.Q.K., S.L., T.N.M.-K., Y.X., K.W. and P.K generated strains. J.J.S performed the data analysis and prepared the manuscript with feedback from other authors. J.J.S. and D.Q.M acquired funding for the completion of this project.

DECLARATION OF INTERESTS

The authors declare no competing interests.

FUNDING

This work was funded by the National Institute of General Medical Sciences (NIGMS) [1R01GM121597-01 to D.Q.M.]. D.Q.M. is also a Damon Runyon-Rachleff Innovator supported (in part) by the Damon Runyon Cancer Research Foundation [DRR-47-17]. J.J.S was supported by an NIH/NIGMS Diversity Supplement [3R01GM121597-02S1]

871 and the W. Burghardt Turner Fellowship. M.A.Q.M. [3R01GM121597-03S1] and F.E.Q.M.
872 [3R01GM121597-04S1] are supported by an NIH/NIGMS Diversity Supplement. A.Q.K.
873 [F31GM128319], R.C.A [1F31GM1283190], and T.N.M.-K. [F31HD100091-01] were
874 supported by the NIH. N.J.P [132969-PF-18-226-01-CSM] was supported by the
875 American Cancer Society (ACS). P.K. [R01NS118078] is supported by the National
876 Institute of Neurological Disorders and Stroke.

877

878 **MATERIALS & METHODS**

879 ***C. elegans* strains and culture conditions**

880 All animals were maintained under standard conditions and cultured at 25°C, except
881 strains containing temperature-sensitive alleles *swsn-1(os22), swsn-4(os13)*, and the
882 uterine-specific RNAi hypersensitive strain used in the chromatin remodeler screen
883 containing the *rrf-3(pk1426)* allele, which were maintained at either 15°C or 20°C (108).
884 The heat shock inducible *cki-1::mTagBFP2* transgene was expressed via incubating
885 animals at 32°C for 2-3 hours in a water bath starting at the P6.p 2-cell VPC stage.
886 Animals were synchronized for experiments through alkaline hypochlorite treatment of
887 gravid adults to isolate eggs (109). In the text and figures, we designate linkage to a
888 promoter through the use of a (p) and fusion of a proteins via a (::) annotation.

889 **Molecular biology and microinjection**

890 SWI/SNF subunits *swsn-4* and *swsn-8* were tagged at their endogenous loci using
891 CRISPR/Cas9 genome editing via microinjection into the early adult hermaphrodite
892 syncytial gonad (110,111). Repair templates were generated as synthetic DNAs from
893 either Integrated DNA Technologies (IDT) as gene blocks (gBlocks) or Twist Biosciences

894 as DNA fragments and cloned into *ccdB* compatible sites in pDD282 by New England
895 Biolabs Gibson assembly (112). Homology arms ranged from 690-1200 bp (see **Tables**
896 **S5** for additional details). sgRNAs were constructed by EcoRV and NheI digestion of the
897 plasmid pDD122. A 230 bp amplicon was generated replacing the sgRNA targeting
898 sequence from pDD122 with a new sgRNA and NEB Gibson assembly was used to
899 generate new sgRNA plasmids (see **Table S5** for additional details). Hermaphrodite
900 adults were co-injected with guide plasmid (50 ng/μL), repair plasmid (50 ng/μL), and an
901 extrachromosomal array marker (pCFJ90, 2.5 ng/μL), and incubated at 25 ºC for several
902 days before screening and floxing protocols associated with the SEC system (112).

903 **RNA interference (RNAi)**

904 All 269 RNAi clones assessed in the chromatin remodeler screen were derived from the
905 commercially available Vidal or Ahringer RNAi libraries. Presence of inserts into the
906 L4440 RNAi vector was confirmed via colony PCR amplification of all L4440 vectors used
907 in the chromatin remodeler screen. Vectors which resulted in penetrant loss of invasion
908 (see **Table S2**) were also sequenced to confirm the identity of the insert targeting
909 chromatin remodeler genes in the L4440 vector using Sanger sequencing at the
910 Genomics Core Facility at Stony Brook University. An RNAi sub-library of SWI/SNF
911 subunits was constructed by cloning 950-1000 bp of synthetic DNA based on cDNA
912 sequences available on WormBase (www.wormbase.org) into the highly efficient T444T
913 RNAi vector (113,114). Synthetic DNAs were generated by Twist Biosciences as DNA
914 fragments and cloned into restriction digested T444T using NEB Gibson Assembly (see
915 **Tables S6** for additional details). For all experiments, synchronized L1 stage animals
916 were directly exposed to RNAi through feeding with bacteria expressing dsRNA (115).

917 **Auxin-mediated degradation**

918 To combine RNAi with the depletion of AID-tagged proteins, 1 mM K-NAA was used, and
919 its effects were analyzed as previously described(116). Briefly, L1 animals were first
920 synchronized by sodium hypochlorite treatment and transferred to NGM plates seeded
921 with the RNAi vector of interest. At the P6.p 1-cell stage, a time in development where
922 the AC has already undergone specification, animals were transferred to RNAi-seeded
923 plates treated with K-NAA. Animals were staged by DIC.

924 **Live cell microscopy**

925 All micrographs included in this manuscript were collected on a Hamamatsu Orca EM-
926 CCD camera mounted on an upright Zeiss AxioImager A2 with a Borealis-modified
927 CSU10 Yokagawa spinning disk scan head using 405nm, 488 nm, and 561 nm Vortran
928 lasers in a VersaLase merge and a Plan-Apochromat 100x/1.4 (NA) Oil DIC objective.
929 MetaMorph software (Molecular Devices) was used for microscopy automation. Several
930 experiments and all RNAi screening were scored using epifluorescence visualized on a
931 Zeiss Axiocam MRM camera, also mounted on an upright Zeiss AxioImager A2 and a
932 Plan-Apochromat 100x/1.4 (NA) Oil DIC objective. Animals were mounted into a drop of
933 M9 on a 5% Noble agar pad containing approximately 10 mM sodium azide anesthetic
934 and topped with a coverslip.

935 **Assessment of AC invasion**

936 Both for the purposes of the CRF RNAi screen and all other experiments AC invasion
937 was scored at the P6.p 4-cell stage, when 100% of wild-type animals exhibit a breach in
938 the BM (14). In strains with the laminin::GFP transgene, an intact green fluorescent barrier
939 under the AC was used to assess invasion. Wild-type invasion is defined as a breach as

940 wide as the basolateral surface of the AC (14). Raw scoring data is available in **Tables**
941 **S1 and S4.**

942 **Image quantification and statistical analyses**

943 Images were processed using Fiji/ImageJ (v.2.1.0/1.53c) (117). Expression levels of
944 GFP::SWSN-4, SWSN-8::GFP, PBRM-1::eGFP, and PBRM-1::mNG::AID were
945 measured by quantifying the mean gray value of AC nuclei, defined as somatic gonad
946 cells near the primary vulva expressing the *cdh-3p::mCherry::moeABD* transgene.
947 Background subtraction was performed by rolling ball background subtraction (size=50).
948 For characterization of experiments involving SWI/SNF endogenous tags and AC GRN
949 TFs::GFP treated with *SWI/SNF(RNAi)* and GFP-targeting nanobody the L3 stage, only
950 animals exhibiting defects in invasion were included in the analysis. Data was normalized
951 to negative control (empty vector) values for the plots in **Fig 3** and **Fig S8**. Quantification
952 of either CDK cell cycle sensor (either DHB::GFP or DHB::2xmKate2) was performed by
953 hand, as previously described (36). Images were overlaid and figures were assembled
954 using Adobe Photoshop 2020 (v. 21.1.2) and Adobe Illustrator 2020 (v. 24.1.2),
955 respectively. Statistical analyses and plotting of data were conducted using RStudio (v.
956 1.2.1335). Statistical significance was determined using either a two-tailed Student's t-
957 test or Fisher's exact probability test. Figure legends specify when each test was used
958 and the p-value cut-off.
959

960 **REFERENCES**

961 1. Rowe RG, Weiss SJ. Breaching the basement membrane: who, when and how?
962 Trends Cell Biol. 2008;18(11):560–74.
963 2. Nourshargh S, Alon R. Leukocyte Migration into Inflamed Tissues. Immunity
964 [Internet]. 2014;41(5):694–707. Available from:
965 http://dx.doi.org/10.1016/j.immuni.2014.10.008
966 3. Medwig TN, Matus DQ. Breaking down barriers: the evolution of cell invasion.
967 Curr Opin Genet Dev [Internet]. 2017;47:33–40. Available from:
968 http://dx.doi.org/10.1016/j.gde.2017.08.003
969 4. Liu Y, Pan YF, Xue YQ, Fang LK, Guo XH, Guo X, et al. UPAR promotes tumor-
970 like biologic behaviors of fibroblast-like synoviocytes through PI3K/Akt signaling
971 pathway in patients with rheumatoid arthritis. Cell Mol Immunol [Internet].
972 2018;15(2):171–81. Available from: http://dx.doi.org/10.1038/cmi.2016.60
973 5. Ye Y, Gao X, Yang N. LncRNA ZFAS1 promotes cell migration and invasion of
974 fibroblast-like synoviocytes by suppression of miR-27a in rheumatoid arthritis.
975 Hum Cell. 2018;31(1):14–21.
976 6. Hanahan D, Weinberg RA. Hallmarks of cancer: The next generation. Cell
977 [Internet]. 2011;144(5):646–74. Available from:
978 http://dx.doi.org/10.1016/j.cell.2011.02.013
979 7. Justus CR, Leffler N, Ruiz-Echevarria M, Yang L V. In vitro cell migration and
980 invasion assays. J Vis Exp. 2014;(88):1–8.
981 8. Li BB, Scott EY, Dean Chamberlain M, Duong BTV, Zhang S, Done SJ, et al. Cell
982 invasion in digital microfluidic microgel systems. Sci Adv. 2020;6(29).

983 9. Eibl G, Reber HA. A xenograft nude mouse model for perineural invasion and
984 recurrence in pancreatic cancer. Pancreas. 2005;31(3):258–62.
985 10. Busuttil RA, Liu DS, Di Costanzo N, Schröder J, Mitchell C, Boussioutas A. An
986 orthotopic mouse model of gastric cancer invasion and metastasis. Sci Rep.
987 2018;8(1):2–9.
988 11. Cheng B, Wang Q, Song Y, Liu Y, Liu Y, Yang S, et al. MIF inhibitor, ISO-1,
989 attenuates human pancreatic cancer cell proliferation, migration and invasion in
990 vitro, and suppresses xenograft tumour growth in vivo. Sci Rep. 2020;10(1):1–10.
991 12. Wen J, Yin P, Li L, Kang G, Ning G, Cao Y, et al. Knockdown of Matrix
992 Metallopeptidase 9 Inhibits Metastasis of Oral Squamous Cell Carcinoma Cells in
993 a Zebrafish Xenograft Model. Biomed Res Int. 2020;2020.
994 13. Guo Y, Fan Y, Pei X. Fangjihuangqi Decoction inhibits MDA-MB-231 cell invasion
995 in vitro and decreases tumor growth and metastasis in triple-negative breast
996 cancer xenografts tumor zebrafish model. Cancer Med. 2020;9(7):2564–78.
997 14. Sherwood DR, Sternberg PW. Anchor cell invasion into the vulval epithelium in C.
998 elegans. Dev Cell. 2003;5(1):21–31.
999 15. Kelley LC, Lohmer LL, Hagedorn EJ, Sherwood DR. Traversing the basement
1000 membrane in vivo: A diversity of strategies. J Cell Biol. 2014;204(3):291–302.
1001 16. Sherwood DR, Butler JA, Kramer JM, Sternberg PW. FOS-1 promotes basement-
1002 membrane removal during anchor-cell invasion in C. elegans. Cell.
1003 2005;121(6):951–62.
1004 17. Hagedorn EJ, Yashiro H, Ziel JW, Ihara S, Wang Z, Sherwood DR. Integrin Acts
1005 Upstream of Netrin Signaling to Regulate Formation of the Anchor Cell's Invasive

1006 Membrane in C. elegans. Dev Cell [Internet]. 2009;17(2):187–98. Available from:
1007 http://dx.doi.org/10.1016/j.devcel.2009.06.006
1008 18. Hagedorn EJ, Kelley LC, Naegeli KM, Wang Z, Chi Q, Sherwood DR. ADF/cofilin
1009 promotes invadopodial membrane recycling during cell invasion in vivo. J Cell
1010 Biol. 2014;204(7):1209–18.
1011 19. Morrissey MA, Jayadev R, Miley GR, Blebea CA, Chi Q, Ihara S, et al. SPARC
1012 Promotes Cell Invasion In Vivo by Decreasing Type IV Collagen Levels in the
1013 Basement Membrane. PLoS Genet. 2016;12(2).
1014 20. Hagedorn EJ, Ziel JW, Morrissey MA, Linden LM, Wang Z, Chi Q, et al. The netrin
1015 receptor DCC focuses invadopodia-driven basement membrane transmigration in
1016 vivo. J Cell Biol. 2013;201(6):903–13.
1017 21. Kelley LC, Chi Q, Cáceres R, Hastie E, Schindler AJ, Matus DQ, et al. Adaptive
1018 F-actin polymerization and localized ATP production drive basement membrane
1019 invasion in the absence of MMPs. Dev Cell. 2019;48(3):313–28.
1020 22. Medwig-Kinney TN, Smith JJ, Palmisano NJ, Tank S, Zhang W, Matus DQ. A
1021 developmental gene regulatory network for C. elegans
1022 anchor cell invasion. Development [Internet]. 2020 Jan 1;147(1):dev185850.
1023 Available from: http://dev.biologists.org/content/147/1/dev185850.abstract
1024 23. Kohrman AQ, Matus DQ. Divide or Conquer: Cell Cycle Regulation of Invasive
1025 Behavior. Trends Cell Biol [Internet]. 2016;27(1):12–25. Available from:
1026 http://dx.doi.org/10.1016/j.tcb.2016.08.003
1027 24. Matus DQ, Lohmer LL, Kelley LC, Schindler AJ, Kohrman AQ, Barkoulas M, et al.
1028 Invasive Cell Fate Requires G1 Cell-Cycle Arrest and Histone Deacetylase-

1029 Mediated Changes in Gene Expression. Dev Cell [Internet]. 2015;35(2):162–74.
1030 Available from: http://dx.doi.org/10.1016/j.devcel.2015.10.002
1031 25. Brand M, Nakka K, Zhu J, Dilworth FJ. Polycomb/Trithorax Antagonism: Cellular
1032 Memory in Stem Cell Fate and Function. Cell Stem Cell [Internet].
1033 2019;24(4):518–33. Available from: https://doi.org/10.1016/j.stem.2019.03.005
1034 26. Simon JA, Tamkun JW. Programming off and on states in chromatin: Mechanisms
1035 of Polycomb and trithorax group complexes. Curr Opin Genet Dev.
1036 2002;12(2):210–8.
1037 27. Kadoch C, Williams RT, Calarco JP, Miller EL, Weber CM, Braun SMG, et al.
1038 Dynamics of BAF – Polycomb complex opposition on heterochromatin in normal
1039 and oncogenic states. Nat Publ Gr [Internet]. 2016;49(2):213–22. Available from:
1040 http://dx.doi.org/10.1038/ng.3734
1041 28. Friman ET, Deluz C, Meireles-Filho ACA, Govindan S, Gardeux V, Deplancke B,
1042 et al. Dynamic regulation of chromatin accessibility by pluripotency transcription
1043 factors across the cell cycle. bioRxiv. 2019;1–28.
1044 29. Ma Y, McKay DJ, Buttitta L. Changes in chromatin accessibility ensure robust cell
1045 cycle exit in terminally differentiated cells. PLoS Biol. 2019;17(9):1–29.
1046 30. Wang S, Tang NH, Lara-Gonzalez P, Zhao Z, Cheerambathur DK, Prevo B, et al.
1047 A toolkit for GFP-mediated tissue-specific protein degradation in C. elegans .
1048 Development. 2017;144(14):2694–701.
1049 31. Bai J, Mei P, Zhang C, Chen F, Li C, Pan Z, et al. BRG1 Is a Prognostic Marker
1050 and Potential Therapeutic Target in Human Breast Cancer. PLoS One.
1051 2013;8(3):1–9.

1052 32. Kadoch C, Hargreaves DC, Hodges C, Elias L, Ho L, Ranish J, et al. a n a ly s i s
1053 Proteomic and bioinformatic analysis of mammalian SWI / SNF complexes
1054 identifies extensive roles in human malignancy. Nat Publ Gr [Internet].
1055 2013;45(6):592–601. Available from: http://dx.doi.org/10.1038/ng.2628
1056 33. Kaufmann B, Wang B, Zhong S, Laschinger M, Patil P, Lu M, et al. BRG1
1057 promotes hepatocarcinogenesis by regulating proliferation and invasiveness.
1058 PLoS One. 2017;12(7):1–14.
1059 34. Bögershausen N, Wollnik B. Mutational Landscapes and Phenotypic Spectrum of
1060 SWI/SNF-Related Intellectual Disability Disorders. Front Mol Neurosci.
1061 2018;11(August):1–18.
1062 35. van der Vaart A, Godfrey M, Portegijs V, van den Heuvel S. Dose-dependent
1063 functions of SWI/SNF BAF in permitting and inhibiting cell proliferation in vivo. Sci
1064 Adv. 2020;6(21).
1065 36. Adikes RC, Kohrman AQ, Martinez MAQ, Palmisano NJ, Smith JJ, Medwig-
1066 Kinney TN, et al. Visualizing the metazoan proliferation-quiescence decision in
1067 vivo. Elife. 2020;9:1–74.
1068 37. Rual JF, Ceron J, Koreth J, Hao T, Nicot AS, Hirozane-Kishikawa T, et al. Toward
1069 improving Caenorhabditis elegans phenome mapping with an ORFeome-based
1070 RNAi library. Genome Res. 2004;14(10 B):2162–8.
1071 38. Kamath RS, Ahringer J. Genome-wide RNAi screening in Caenorhabditis
1072 elegans. Methods. 2003;30(4):313–21.
1073 39. Matus DQ, Li X-Y, Durbin S, Agarwal D, Chi Q, Weiss SJ, et al. In vivo
1074 identification of regulators of cell invasion across basement membranes. Sci

1075 Signal [Internet]. 2010;3(120):ra35. Available from:
1076 http://www.pubmedcentral.nih.gov/articlerender.fcgi?artid=3917318&tool=pmcentr
1077 ez&rendertype=abstract
1078 40. W W. The SWI / SNF Family of ATP-Dependent Chromatin Remodelers : Similar
1079 Mechanisms for Diver Function. In: Workman JL, editor. Protein Complexes that
1080 Modify Chromatin. Springer-Verlag Berling Heidelberg; 2003. p. 144–65.
1081 41. Sawa H, Kouike H, Okano H. Components of the SWI/SNF complex are required
1082 for asymmetric cell division in C. elegans. Mol Cell. 2000;6(3):617–24.
1083 42. Cui M, Fay DS, Han M. Lin-35/Rb cooperates with the SWI/SNF complex to
1084 control Caenorhabditis elegans larval development. Genetics. 2004;167(3):1177–
1085 85.
1086 43. Large EE, Mathies LD. Caenorhabditis elegans SWI/SNF subunits control
1087 sequential developmental stages in the somatic gonad. G3 (Bethesda) [Internet].
1088 2014;4(3):471–83. Available from:
1089 http://www.pubmedcentral.nih.gov/articlerender.fcgi?artid=3962486&tool=pmcentr
1090 ez&rendertype=abstract
1091 44. Ertl I, Porta-De-La-Riva M, Gómez-Orte E, Rubio-Peña K, Corrales D, Cornes E,
1092 et al. Functional interplay of two paralogs encoding SWI/SNF chromatin-
1093 remodeling accessory subunits during Caenorhabditis elegans development.
1094 Genetics. 2016;202(3):961–75.
1095 45. Cenik BK, Shilatifard A. COMPASS and SWI/SNF complexes in development and
1096 disease. Nat Rev Genet [Internet]. 2021;22(1):38–58. Available from:
1097 http://dx.doi.org/10.1038/s41576-020-0278-0

1098 46. Kadoch C, Crabtree GR. Mammalian SWI/SNF chromatin remodeling complexes
1099 and cancer: Mechanistic insights gained from human genomics. Sci Adv
1100 [Internet]. 2015;1(5):e1500447–e1500447. Available from:
1101 http://advances.sciencemag.org/cgi/doi/10.1126/sciadv.1500447
1102 47. Nickerson JA, Wu Q, Imbalzano AN. Mammalian SWI/SNF enzymes and the
1103 epigenetics of tumor cell metabolic reprogramming. Front Oncol. 2017;7(APR):1–
1104 9.
1105 48. Mittal P, Roberts CWM. The SWI/SNF complex in cancer — biology, biomarkers
1106 and therapy. Nat Rev Clin Oncol [Internet]. 2020;17(7):435–48. Available from:
1107 http://dx.doi.org/10.1038/s41571-020-0357-3
1108 49. Muchardt C, Yaniv M. When the SWI/SNF complex remodels...the cell cycle.
1109 Oncogene. 2001;20(24):3067–75.
1110 50. Nagl NG, Zweitzig DR, Thimmapaya B, Beck GR, Moran E. The c-myc gene is a
1111 direct target of mammalian SWI/SNF-related complexes during differentiation-
1112 associated cell cycle arrest. Cancer Res. 2006;66(3):1289–93.
1113 51. Moshkin YM, Mohrmann L, van Ijcken WFJ, Verrijzer CP. Functional
1114 Differentiation of SWI/SNF Remodelers in Transcription and Cell Cycle Control.
1115 Mol Cell Biol [Internet]. 2007;27(2):651–61. Available from:
1116 http://mcb.asm.org/cgi/doi/10.1128/MCB.01257-06
1117 52. Ruijtenberg S, Van Den Heuvel S. G1/S Inhibitors and the SWI/SNF Complex
1118 Control Cell-Cycle Exit during Muscle Differentiation. Cell [Internet].
1119 2015;162(2):300–13. Available from: http://dx.doi.org/10.1016/j.cell.2015.06.013
1120 53. Innis SM, Cabot B. GBAF, a small BAF sub-complex with big implications: a

1121 systematic review. Epigenetics and Chromatin [Internet]. 2020;13(1):1–18.
1122 Available from: https://doi.org/10.1186/s13072-020-00370-8
1123 54. Son EY, Crabtree GR. The role of BAF (mSWI/SNF) complexes in mammalian
1124 neural development. Am J Med Genet C Semin Med Genet. 2014;(650).
1125 55. Mathies LD, Blackwell GG, Austin MK, Edwards AC, Riley BP, Davies AG, et al.
1126 SWI/SNF chromatin remodeling regulates alcohol response behaviors in
1127 Caenorhabditis elegans and is associated with alcohol dependence in humans.
1128 Proc Natl Acad Sci U S A [Internet]. 2015;112(10):3032–7. Available from:
1129 /pmc/articles/PMC4364201/?report=abstract
1130 56. Kuzmanov A, Karina EI, Kirienko N V., Fay DS. The Conserved PBAF
1131 Nucleosome-Remodeling Complex Mediates the Response to Stress in
1132 Caenorhabditis elegans. Mol Cell Biol. 2014;34(6):1121–35.
1133 57. Hayes GD, Riedel CG, Ruvkun G. The Caenorhabditis elegans somi-1 zinc finger
1134 protein and SWI/SNF promote regulation of development by the mir-84
1135 microRNA. Genes Dev. 2011;25(19):2079–92.
1136 58. Shibata Y, Uchida M, Takeshita H, Nishiwaki K, Sawa H. Multiple functions of
1137 PBRM-1/Polybromo- and LET-526/Osa-containing chromatin remodeling
1138 complexes in C. Elegans development. Dev Biol [Internet]. 2012;361(2):349–57.
1139 Available from: http://dx.doi.org/10.1016/j.ydbio.2011.10.035
1140 59. Weinberg P, Flames N, Sawa H, Garriga G, Hobert O. The SWI/SNF chromatin
1141 remodeling complex selectively affects multiple aspects of serotonergic neuron
1142 differentiation. Genetics. 2013;194(1):189–98.
1143 60. Riedel CG, Dowen RH, Lourenco GF, Natalia V, Heimbucher T, West JA, et al.

1144 DAF-16/FOXO employs the chromatin remodeller SWI/SNF to promote stress
1145 resistance and longevity. 2013;15(5):491–501.
1146 61. Kipreos ET, van den Heuvel S. Developmental Control of the Cell Cycle: Insights
1147 from Caenorhabditis elegans. Genetics. 2019;211(3):797–829.
1148 62. Sturm Á, Saskoï É, Tibor K, Weinhardt N, Vellai T. Highly efficient RNAi and
1149 Cas9-based auto-cloning systems for C. Elegans research. Nucleic Acids Res.
1150 2018;46(17):1–13.
1151 63. Dickinson DJ, Goldstein B. CRISPR-based methods for caenorhabditis elegans
1152 genome engineering. Genetics. 2016;202(3):885–901.
1153 64. Mashtalir N, D'Avino AR, Michel BC, Luo J, Pan J, Otto JE, et al. Modular
1154 Organization and Assembly of SWI/SNF Family Chromatin Remodeling
1155 Complexes. Cell [Internet]. 2018;175(5):1272-1288.e20. Available from:
1156 https://doi.org/10.1016/j.cell.2018.09.032
1157 65. Rago F, DiMare MT, Elliott GN, Ruddy DA, Sovath S, Kerr G, et al. Degron
1158 mediated BRM/SMARCA2 depletion uncovers novel combination partners for
1159 treatment of BRG1/SMARCA4-mutant cancers. Biochem Biophys Res Commun
1160 [Internet]. 2019;508(1):109–16. Available from:
1161 https://doi.org/10.1016/j.bbrc.2018.09.009
1162 66. Ziel JW, Matus DQ, Sherwood DR. An expression screen for RhoGEF genes
1163 involved in C. elegans gonadogenesis. Gene Expr Patterns [Internet].
1164 2009;9(6):397–403. Available from:
1165 http://www.nature.com/doifinder/10.1038/jid.2014.371
1166 67. Rimann I, Hajnal A. Regulation of anchor cell invasion and uterine cell fates by

1167 the egl-43 Evi-1 proto-oncogene in Caenorhabditis elegans. Dev Biol.
1168 2007;308(1):187–95.
1169 68. Deng T, Stempor P, Appert A, Daube M, Ahringer J, Hajnal A, et al. The
1170 caenorhabditis elegans homolog of the evi1 proto-oncogene, egl-43, coordinates
1171 G1 cell cycle arrest with pro-invasive gene expression during anchor cell invasion.
1172 PLoS Genet [Internet]. 2020;16(3). Available from:
1173 http://dx.doi.org/10.1371/journal.pgen.1008470
1174 69. Hwang BJ, Meruelo AD, Sternberg PW. C. elegans EVI1 proto-oncogene, EGL-
1175 43, is necessary for Notch-mediated cell fate specification and regulates cell
1176 invasion. Development. 2007;134(4):669–79.
1177 70. Spencer SL, Cappell SD, Tsai F, Overton KW, Wang L, Meyer T. The
1178 Proliferation-Quiescence Decision Is Controlled by a Bifurcation in CDK2 Activity
1179 at Mitotic Exit. 2013;155(2):369–83.
1180 71. Kimble J, Hirsh D. The postembryonic cell lineages of the hermaphrodite and
1181 male gonads in Caenorhabditis elegans. Dev Biol. 1979;70(2):396–417.
1182 72. Newman AP, White JG, Sternberg PW. Morphogenesis of the C. elegans
1183 hermaphrodite uterus. Development [Internet]. 1996 Nov 1;122(11):3617 LP –
1184 3626. Available from: http://dev.biologists.org/content/122/11/3617.abstract
1185 73. Cao Y, Cairns BR, Kornberg RD, Laurent BC. Sfh1p, a component of a novel
1186 chromatin-remodeling complex, is required for cell cycle progression. Mol Cell
1187 Biol. 1997;17(6):3323–34.
1188 74. Angus-Hill ML, Schlichter A, Roberts D, Erdjument-Bromage H, Tempst P, Cairns
1189 BR. A Rsc3/Rsc30 zinc cluster dimer reveals novel roles for the chromatin

1190 remodeler RSC in gene expression and cell cycle control. Mol Cell.
1191 2001;7(4):741–51.
1192 75. Zhang L, Ward JD, Cheng Z, Dernburg AF. The auxin-inducible degradation (AID)
1193 system enables versatile conditional protein depletion in C. elegans. Development
1194 [Internet]. 2015;142(24):4374–84. Available from:
1195 http://dev.biologists.org/content/142/24/4374.abstract
1196 76. Martinez MAQ, Kinney BA, Medwig-Kinney TN, Ashley G, Ragle JM, Johnson L,
1197 et al. Rapid degradation of C. elegans proteins at single-cell resolution with a
1198 synthetic auxin. G3 (Bethesda). 2020;10(January):267–80.
1199 77. Wang L, Shen W, Lei S, Matus D, Sherwood D, Wang Z. MIG-10 (Lamellipodin)
1200 stabilizes invading cell adhesion to basement membrane and is a negative
1201 transcriptional target of EGL-43 in C. elegans. Biochem Biophys Res Commun
1202 [Internet]. 2014;452(3):328–33. Available from:
1203 http://dx.doi.org/10.1016/j.bbrc.2014.08.049
1204 78. Sherwood, DR., Plastino J. Invading , Leading and Navigating Cells in
1205 Caenorhabditis elegans : Insights into Cell Movement in Vivo. In: WormBook : the
1206 online review of C elegans biology. 2018. p. 53–78.
1207 79. Ribeiro-Silva C, Vermeulen W, Lans H. SWI/SNF: Complex complexes in genome
1208 stability and cancer. DNA Repair. 2019.
1209 80. Lu P, Roberts CW. The SWI/SNF tumor suppressor complex. Nucleus [Internet].
1210 2013;4(5):374–8. Available from:
1211 http://www.tandfonline.com/doi/abs/10.4161/nucl.26654
1212 81. Hargreaves DC, Crabtree GR. ATP-dependent chromatin remodeling: Genetics,

1213 genomics and mechanisms. Cell Res [Internet]. 2011;21(3):396–420. Available
1214 from: http://dx.doi.org/10.1038/cr.2011.32
1215 82. Yang YF, Pan YH, Tian QH, Wu DC, Su SG. CBX1 Indicates Poor Outcomes and
1216 Exerts Oncogenic Activity in Hepatocellular Carcinoma. Transl Oncol [Internet].
1217 2018;11(5):1110–8. Available from: https://doi.org/10.1016/j.tranon.2018.07.002
1218 83. Bracken AP, Brien GL, Verrijzer CP. Dangerous liaisons: interplay between
1219 SWI/SNF, NuRD, and Polycomb in chromatin regulation and cancer. Genes Dev
1220 [Internet]. 2019;1–24. Available from:
1221 http://genesdev.cshlp.org/lookup/doi/10.1101/gad.326066.119
1222 84. Wang G, Tang J, Zhan W, Zhang R, Zhang M, Liao D, et al. CBX8 suppresses
1223 tumor metastasis via repressing snail in esophageal squamous cell carcinoma.
1224 Theranostics. 2017;7(14):3478–88.
1225 85. Ma J, Zhan Y, Xu Z, Li Y, Luo A, Ding F, et al. ZEB1 induced miR-99b/let-7e/miR-
1226 125a cluster promotes invasion and metastasis in esophageal squamous cell
1227 carcinoma. Cancer Lett. 2017;398:37–45.
1228 86. Zhou D.X., Zhou D., Zhan S.Q., Wang P., Qin K., Gan W. LXF. Inhibition of
1229 JMJD6 expression reduces the proliferation, migration and invasion of
1230 neuroglioma stem cells. Neoplasma. 2017;64(5).
1231 87. Bondy-Chorney E, Baldwin RM, Didillon A, Chabot B, Jasmin BJ, Côté J. RNA
1232 binding protein RALY promotes Protein Arginine Methyltransferase 1 alternatively
1233 spliced isoform v2 relative expression and metastatic potential in breast cancer
1234 cells. Int J Biochem Cell Biol [Internet]. 2017;91(March):124–35. Available from:
1235 http://dx.doi.org/10.1016/j.biocel.2017.07.008

1236 88. Zhong S, Yan H, Chen Z, Li Y, Shen Y, Wang Y, et al. Overexpression of TAF1L
1237 promotes cell proliferation, migration and invasion in esophageal squamous cell
1238 carcinoma. J Cancer. 2019;10(4):979–89.
1239 89. Gillison ML, Akagi K, Xiao W, Jiang B, Pickard RKL, Li J, et al. Human
1240 papillomavirus and the landscape of secondary genetic alterations in oral cancers.
1241 Genome Res. 2019;29(1):1–17.
1242 90. Yang L, Zeng W, Sun H, Huang F, Yang C, Cai X, et al. Bioinformatical Analysis
1243 of Gene Expression Omnibus Database Associates TAF7/CCNB1, TAF7/CCNA2,
1244 and GTF2E2/CDC20 Pathways with Glioblastoma Development and Prognosis.
1245 World Neurosurg [Internet]. 2020;138:e492–514. Available from:
1246 https://doi.org/10.1016/j.wneu.2020.02.159
1247 91. Herpel E, Rieker RJ, Dienemann H, Muley T, Meister M, Hartmann A, et al.
1248 SMARCA4 and SMARCA2 deficiency in non–small cell lung cancer:
1249 immunohistochemical survey of 316 consecutive specimens. Ann Diagn Pathol
1250 [Internet]. 2017;26:47–51. Available from:
1251 http://dx.doi.org/10.1016/j.anndiagpath.2016.10.006
1252 92. Shibata Y, Uchida M, Takeshita H, Nishiwaki K, Sawa H. Multiple functions of
1253 PBRM-1/Polybromo- and LET-526/Osa-containing chromatin remodeling
1254 complexes in C. Elegans development. Dev Biol [Internet]. 2012;361(2):349–57.
1255 Available from: http://dx.doi.org/10.1016/j.ydbio.2011.10.035
1256 93. Zhang Z, Wang F, Du C, Guo H, Ma L, Liu X, et al. BRM/SMARCA2 promotes the
1257 proliferation and chemoresistance of pancreatic cancer cells by targeting
1258 JAK2/STAT3 signaling. Cancer Lett [Internet]. 2017;402:213–24. Available from:

1259 http://dx.doi.org/10.1016/j.canlet.2017.05.006
1260 94. Wu RC, Wang TL, Shih IM. The emerging roles of ARID1A in tumor suppression.
1261 Cancer Biol Ther. 2014;15(6):655–64.
1262 95. Clapier CR, Iwasa J, Cairns BR, Peterson CL. Mechanisms of action and
1263 regulation of ATP-dependent chromatin-remodelling complexes. Nat Publ Gr
1264 [Internet]. 2017; Available from: http://dx.doi.org/10.1038/nrm.2017.26
1265 96. Vries RGJ, Bezrookove V, Zuijderduijn LMP, Kia SK, Houweling A, Oruetxebarria
1266 I, et al. Cancer-associated mutations in chromatin remodeler hSNF5 promote
1267 chromosomal instability by compromising the mitotic checkpoint. Genes Dev.
1268 2005;19(6):665–70.
1269 97. Kadoch C, Copeland RA, Keilhack H. PRC2 and SWI/SNF Chromatin
1270 Remodeling Complexes in Health and Disease. Biochemistry. 2016;55(11):1600–
1271 14.
1272 98. Shain AH, Pollack JR. The Spectrum of SWI/SNF Mutations, Ubiquitous in
1273 Human Cancers. PLoS One. 2013;8(1).
1274 99. Fernando TM, Piskol R, Bainer R, Sokol ES, Trabucco SE, Zhang Q, et al.
1275 Functional characterization of SMARCA4 variants identified by targeted exome-
1276 sequencing of 131,668 cancer patients. Nat Commun [Internet]. 2020;11(1):1–13.
1277 Available from: http://dx.doi.org/10.1038/s41467-020-19402-8
1278 100. Dutta A, Sardiu M, Gogol M, Gilmore J, Zhang D, Florens L, et al. Composition
1279 and Function of Mutant Swi/Snf Complexes. Cell Rep [Internet]. 2017;18(9):2124–
1280 34. Available from: http://linkinghub.elsevier.com/retrieve/pii/S2211124717301158
1281 101. Hoffman GR, Rahal R, Buxton F, Xiang K, McAllister G, Frias E, et al. Functional

1282 epigenetics approach identifies BRM/SMARCA2 as a critical synthetic lethal
1283 target in BRG1-deficient cancers. Proc Natl Acad Sci U S A. 2014;111(8):3128–
1284 33.
1285 102. Sasaki M, Ogiwara H. Synthetic lethal therapy based on targeting the vulnerability
1286 of SWI/SNF chromatin remodeling complex-deficient cancers. Cancer Sci.
1287 2020;111(3):774–82.
1288 103. Reisman DN, Sciarrotta J, Wang W, Funkhouser WK, Weissman BE. Loss of
1289 BRG1/BRM in human lung cancer cell lines and primary lung cancers: Correlation
1290 with poor prognosis. Cancer Res. 2003;63(3):560–6.
1291 104. Marquez-Vilendrer SB, Rai SK, Gramling SJ, Lu L, Reisman DN. Loss of the
1292 SWI/SNF atpase subunits BRM and BRG1 drives lung cancer development.
1293 Oncoscience. 2016;3(11–12):322–36.
1294 105. Sulston JE, Horvitz HR. Post-embryonic cell lineages of the nematode,
1295 Caenorhabditis elegans. Dev Biol. 1977;56(1):110–56.
1296 106. Katsanos D, Barkoulas M. Tissue-specific transcription factor target identification
1297 in the Caenorhabditis elegans epidermis using targeted DamID. bioRxiv [Internet].
1298 2020; Available from: https://doi.org/10.1101/2020.12.17.423252
1299 107. Morrissey MA, Keeley DP, Hagedorn EJ, McClatchey STH, Chi Q, Hall DH, et al.
1300 B-LINK: A Hemicentin, Plakin, and Integrin-Dependent Adhesion System that
1301 Links Tissues by Connecting Adjacent Basement Membranes. Dev Cell.
1302 2014;31(3):319–31.
1303 108. Simmer F, Tijsterman M, Parrish S, Koushika SP, Nonet ML, Fire A, et al. Loss of
1304 the putative RNA-directed RNA polymerase RRF-3 makes C. Elegans

1305 hypersensitive to RNAi. Curr Biol. 2002;12(15):1317–9.
1306 109. Porta-de-la-Riva M, Fontrodona L, Villanueva A, Cerón J. Basic Caenorhabditis
1307 elegans methods: Synchronization and observation. J Vis Exp. 2012;(64):1–9.
1308 110. Dickinson DJ, Ward JD, Reiner DJ, Goldstein B. Engineering the Caenorhabditis
1309 elegans genome using Cas9-triggered homologous recombination. Nat Methods.
1310 2013;10(10):1028–34.
1311 111. Dickinson DJ, Goldstein B. CRISPR-based methods for caenorhabditis elegans
1312 genome engineering. Genetics. 2016;202(3):885–901.
1313 112. Dickinson DJ, Pani AM, Heppert JK, Higgins CD, Goldstein B. Streamlined
1314 genome engineering with a self-excising drug selection cassette. Genetics.
1315 2015;200(4):1035–49.
1316 113. Grove C, Cain S, Chen WJ, Davis P, Harris T, Howe K, et al. Using WormBase, a
1317 genome biology resource for Caenorhabditis elegans and related nematodes.
1318 Methods Mol Biol. 2018;1757:399–470.
1319 114. Sturm Á, Saskoi É, Tibor K, Weinhardt N, Vellai T. Highly efficient RNAi and
1320 Cas9-based auto-cloning systems for C. elegans research. Nucleic Acids Res.
1321 2018;46(17):e105.
1322 115. Conte Jr. D, T. Macneil L, J. M. Walhout A, C. Mello C. RNA Interference in
1323 Caenorhabditis Elegans. Current Protocol in Microbiology. 2015. 1–39 p.
1324 116. Martinez M, Matus D. Auxin-mediated Protein Degradation in Caenorhabditis
1325 elegans. Bio-Protocol. 2020;10(8).
1326 117. Schindelin J, Arganda-Carreras I, Frise E, Kaynig V, Longair M, Pietzsch T, et al.
1327 Fiji: An open-source platform for biological-image analysis. Nat Methods.

1328 2012;9(7):676–82.

1329

SUPPLEMENTAL FIGURES

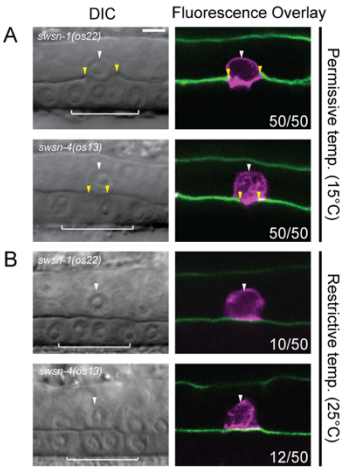

Figure S1. AC invasion is disrupted in temperature sensitive SWI/SNF hypomorphs. Single planes of confocal z-stacks representing AC invasion in *swsn-1(os22) and swsn-4(os13)* temperature sensitive mutants with fluorescently labeled AC (magenta, *cdh-3>mCherry::moeABD*) and BM (green, *laminin::GFP*) scored at the permissive temperature **(A)** and restrictive temperature **(B)**. Significant loss of invasion was seen in both *swsn-1(os22)* (20% loss of invasion) and *swsn-4(os13)* (24% loss of invasion) hypomorphic^{ts} strains when grown at the restrictive temperature 25°C and assessed at the P6.p 4-cell 1° VPC stage **(B)**.

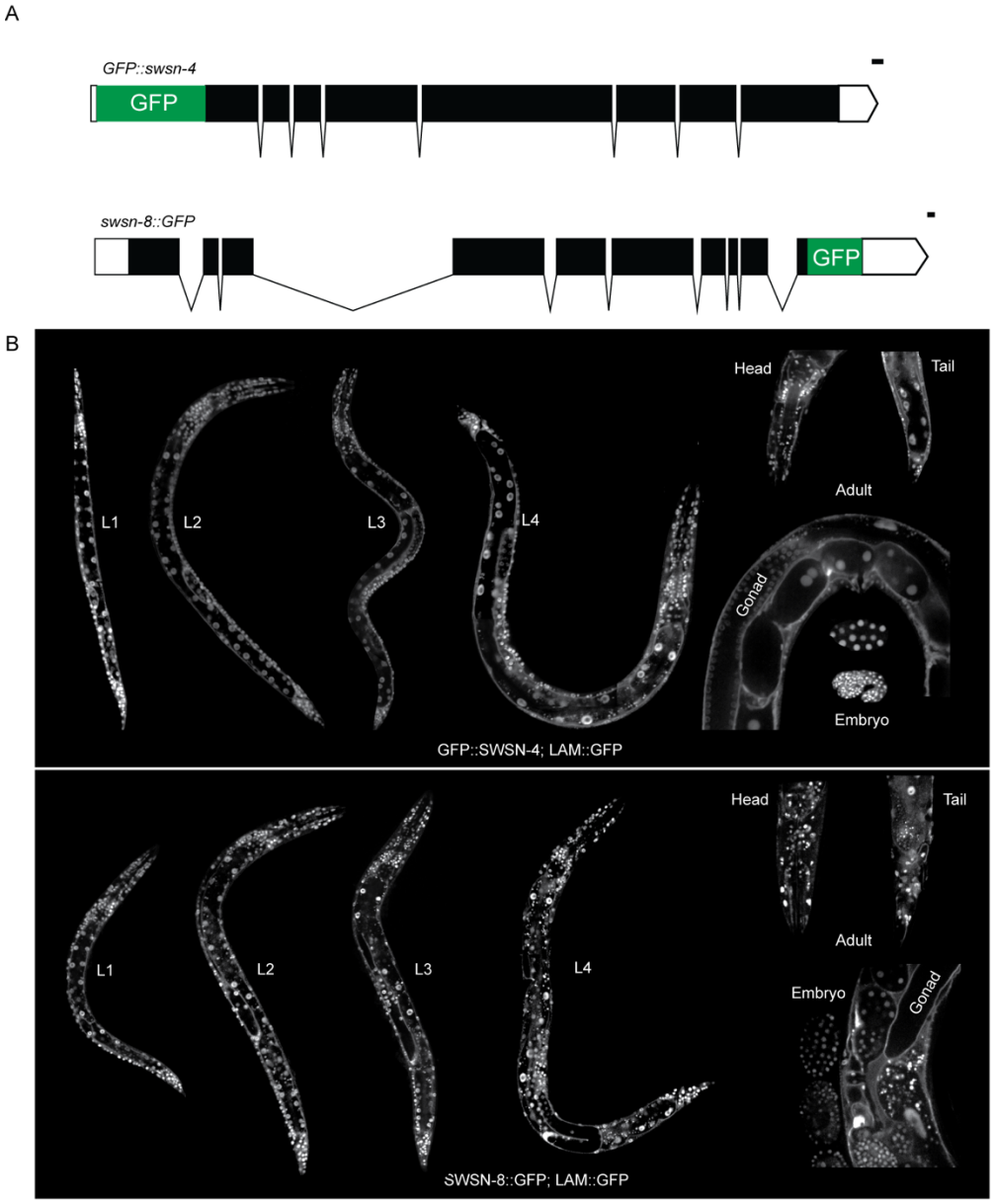

Figure S2. Endogenous SWSN-4::GFP and SWSN-8::GFP are ubiquitously expressed. (A) Schematic (from http://wormweb.org/exonintron) depicting GFP insertion into the endogenous N and C termini of *swsn-4* (top) and *swsn-8* (bottom), respectively. Scale bar, 100 bp. **(B)** Expression of endogenously GFP-labeled SWI/SNF ATPase SWSN-4 protein and BM (*laminin::GFP*) in all larval stages (L1-L4), adult animals, and embryos. **(C)** Expression of endogenously GFP-labeled SWI/SNF ATPase SWSN-4 protein and BM (*laminin::GFP*) in all larval stages (L1-L4), adult animals, and embryos. Images in B-C are not to scale.

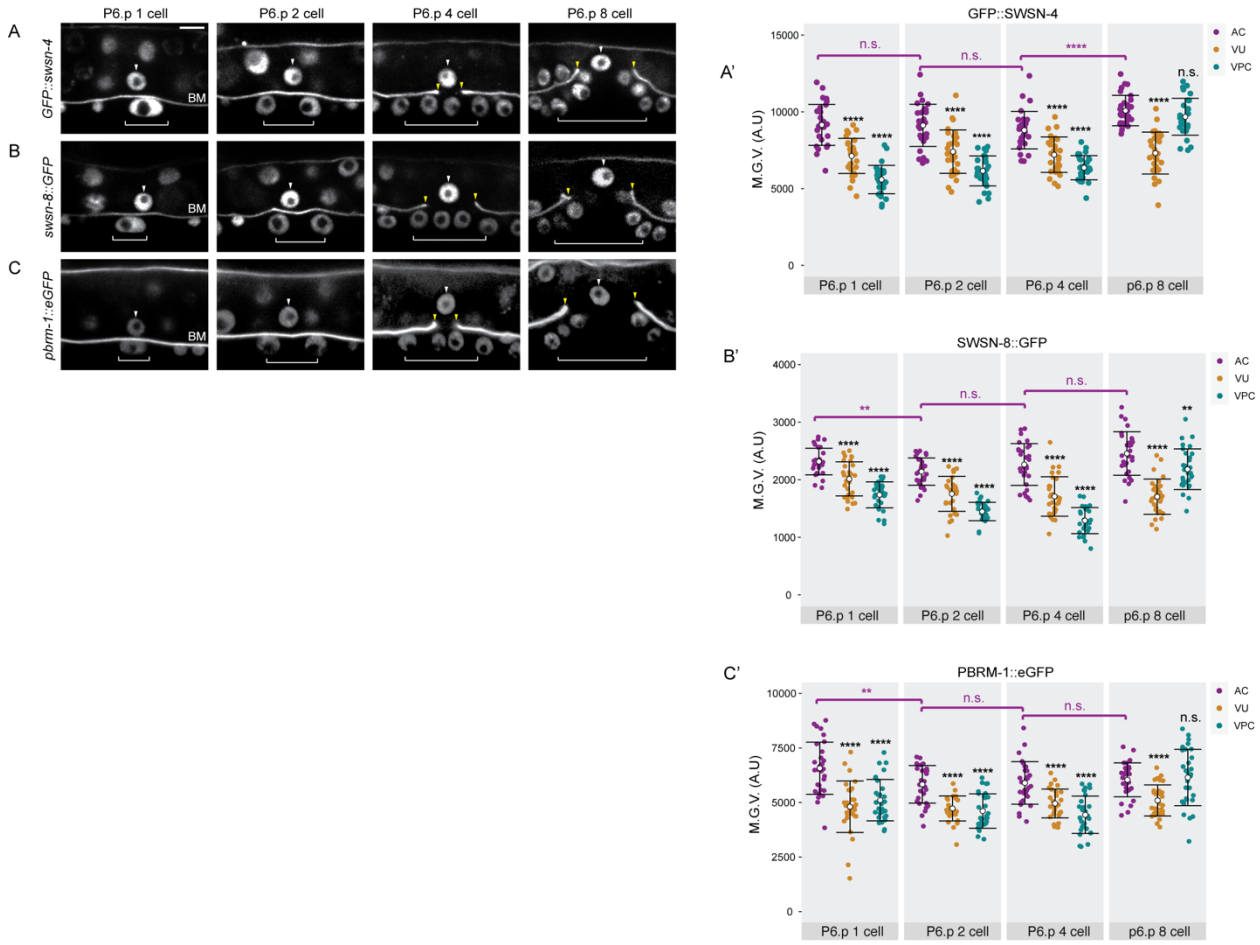

1335

1336

Figure S3. Fluorescent knock-ins express in the AC pre-, during, and post-invasion. Fluorescent micrographs depicting expression of SWSN-4::GFP **(A),** SWSN-8::**GFP (B)**, and PBRM-1::eGFP **(C)** in the AC, VU, and VPCs from the P6.p 1 cell to the P6.p 8 cell stages of development and corresponding quantifications. White arrowheads indicate AC, White brackets indicate 1° VPC stage. **(A'-C')** Quantification of endogenous GFP expression of SWI/SNF subunit in the AC, VU, and VPC over time. Statistical comparisons were made between the expression of each SWI/SNF subunit in the AC over time (magenta bracket and asterisks) or between the expression of each subunit in the AC relative to the expression of the same subunit in the neighboring VPCs or VUs at the same time (black asterisks) using Student's *t*-test (n≥30 for each stage and subunit; p values are displayed above compared groups). n.s. not significant.

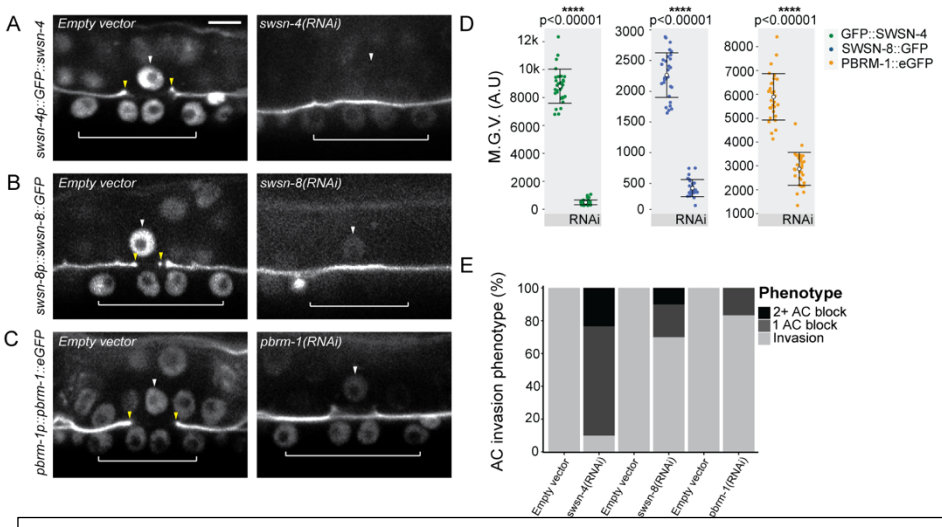

Figure S4. Improved SWI/SNF RNAi significantly knocks down SWI/SNF expression in the AC. Fluorescent micrographs depicting BM (*laminin::GFP*) and expression of SWSN-4::GFP **(A)**, SWSN-8::GFP **(B)**, and PBRM-1::eGFP **(C)** in the AC in animals fed empty vector control (left) or RNAi targeting the endogenous allele (right). White arrowheads indicate AC(s), yellow arrowheads indicate boundaries of breach in BM, and white brackets indicate 1 VPCs. **(D)** Corresponding quantifications of fluorescent expression. Statistical comparisons were made between the expression of each SWI/SNF subunit in the AC in control and RNAi-treated animals using Student's *t*-test (n≥30 for each stage and subunit; p values are displayed above compared data). **(E)** Stacked bar chart showing percentage of AC invasion defects corresponding to each treatment, binned by AC phenotype (n≥30 animals per condition).

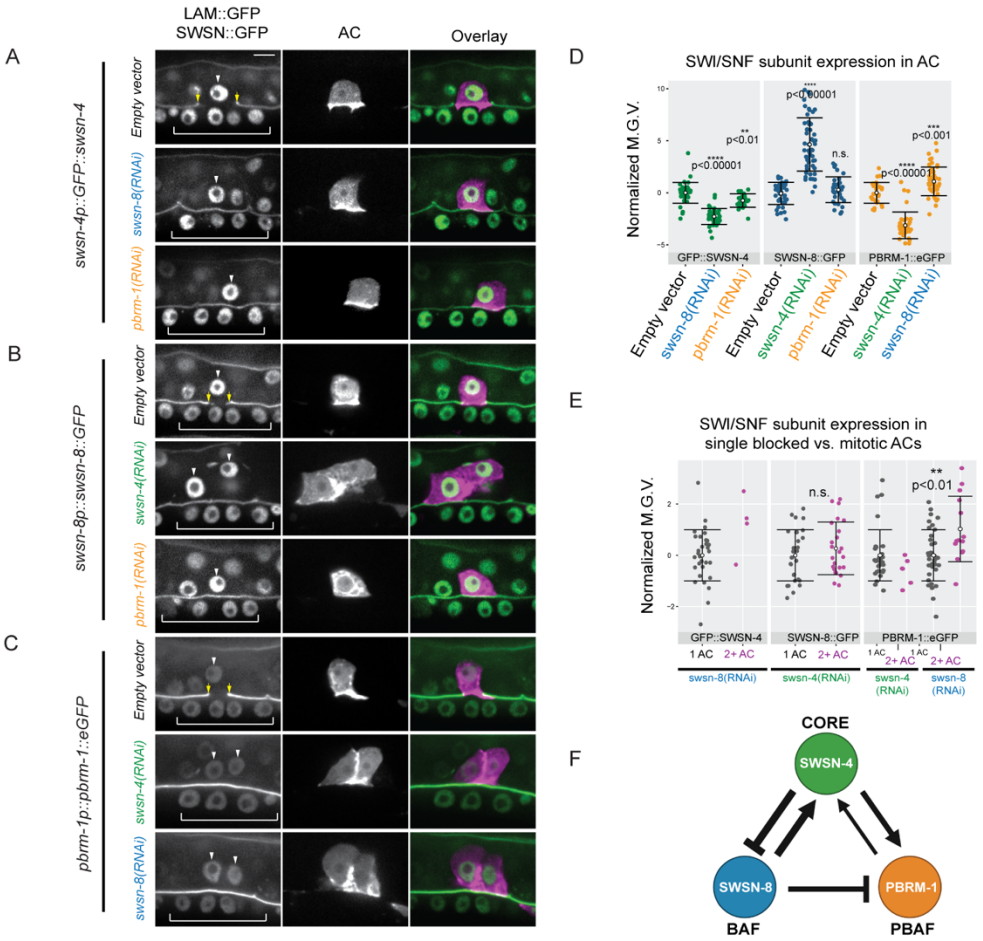

1339

1340 **Figure S5. SWI/SNF subunits exhibit intra-complex and inter-assembly regulation. (A-C)** Representative fluorescence micrographs depicting endogenous GFP expression of individual SWI/SNF subunits representative of the core (*swsn-4*, **A**), BAF assembly (*swsn-8,* **B**), and PBAF assembly (*pbrm-1*, **C**) in the AC (*cdh-3p::mCherry::*moeABD) following treatment with targeting either SWI/SNF assembly **(A),** or the core ATPase and alternative SWI/SNF assembly **(B-C)**. White arrowheads indicate AC(s), yellow arrowheads indicate boundaries of breach in BM, and white brackets indicate 1 VPCs. **(D)** Quantification of fluorescence expression (mean gray value) of endogenous subunits in each condition. Statistical comparisons were made between the expression of each SWI/SNF subunit in the AC in control and RNAi-treated animals using Student's *t*-test (n≥30 for each stage and subunit; p values are displayed above compared data). n.s. not significant**. (E)** Quantification of fluorescence expression of endogenous GFP-tagged subunits of non-invasive ACs following loss of expression of alternative SWI/SNF subunits, binned per RNAi treatment by phenotype into single non-invasive AC (1AC) and mitotic non-invasive AC (2+ AC). Statistical comparisons (Student's *t*-test; p values are displayed above compared data) were limited to conditions with n>10 ACs in each phenotype. n.s. not significant. **(F)** Schematic summary of SWI/SNF core and assembly auto and cross regulation.

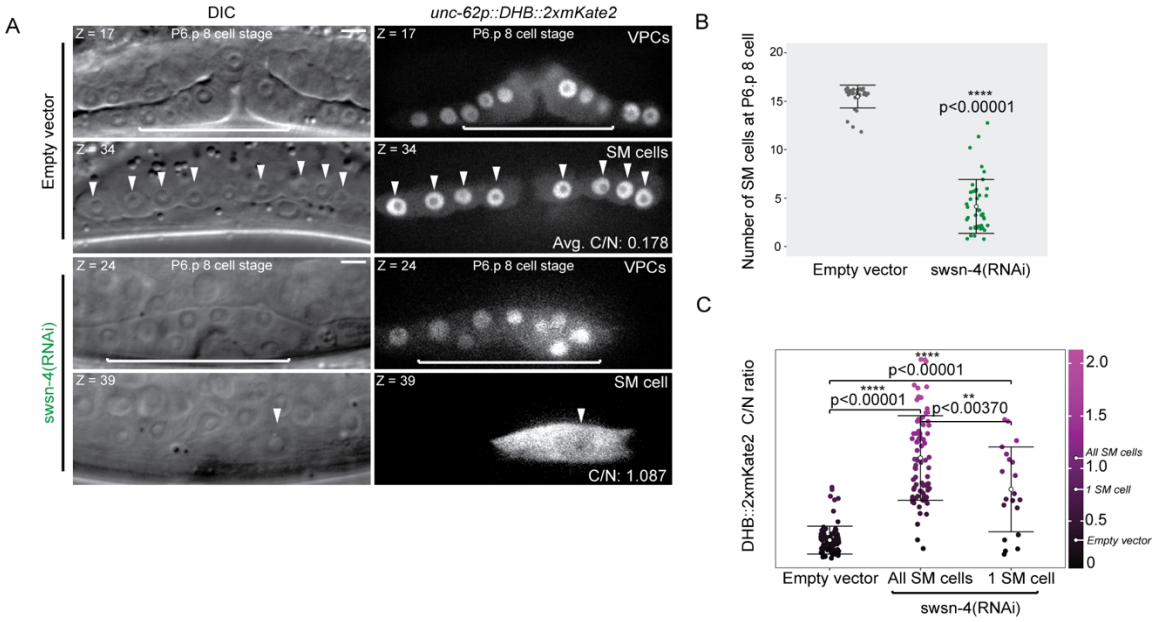

Figure S6. Improved *swsn-4* RNAi recapitulates SWI/SNF ATPase null phenotype in the sex myoblasts. (A) Single confocal z-planes depicting DIC (left) and expression of lineage-restricted CDK sensor (*unc-62>DHB::2xmKate2*, right) in the vulva and SM cells at the P6.p 8 cell stage corresponding to the stage when wild-type SM cells differentiate and exit the cell cycle. Animals were treated with empty vector control (top) or *swsn-4(RNAi)* (bottom). All representative images in each treatment are derived from the same z-stack from the same animal in the corresponding z-plane (top-left). Average or individual C/N CDK sensor ratios are listed in the bottom-right of corresponding panels. White arrowheads indicate individual SM cells. White brackets indicate 1° VPCs. **(B)** Quantification of the number of SM cells present at the P6.p 8 cell stage in control (black) and *swsn-4(RNAi)* treated animals (SMs arrive on both left and right side of vulva at the P6.p 8 cell, green; SMs arrive on either left or right side of vulva at the P6.p 8 cell stage, blue). **(C)** C/N CDK sensor ratios for SM cells in each treatment. Mean C/N ratio is represented by colored open circles and correspond to numbers of the same color. Gradient scale depicts cell cycle state as determined by quantification of each AC in all treatments (n≥30 animals per treatment), with dark-black depicting differentiation into G_0/G_1 and lighter-magenta depicting G_2 cell cycle states.

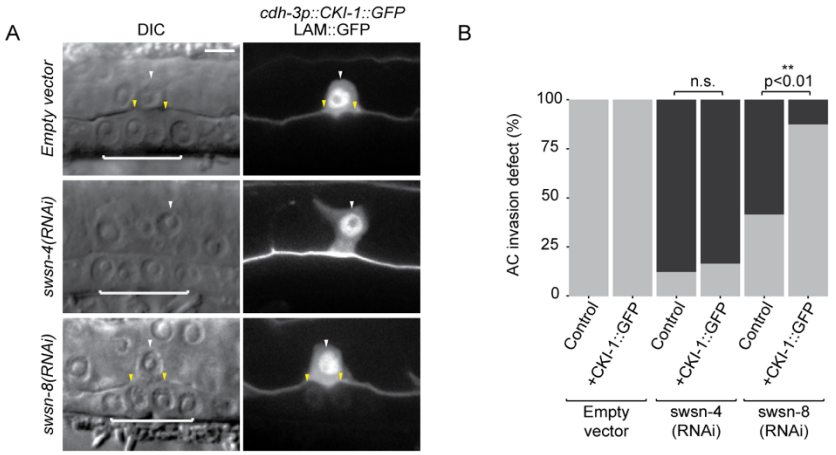

Figure S7. AC-specific expression of CKI-1 rescues invasion in BAF-depleted ACs. (A) DIC (left) and fluorescent (right) images depicting BM (*laminin::GFP*) and AC-specific CKI-1 (*cdh-3>CKI-1::GFP*) in empty vector control animals (top) and animals treated with *swsn-4(RNAi)* (middle) or *swsn-8(RNAi)* (bottom). **(B)** Stacked bar chart showing quantification of percentage of AC invasion defects corresponding to each treatment (n≥30 animals per condition, p values for Fisher's exact test comparing invasion penetrance in control animals and animals with the rescue transgene (+CKI-1::GFP) are displayed above black brackets).

1343

1344

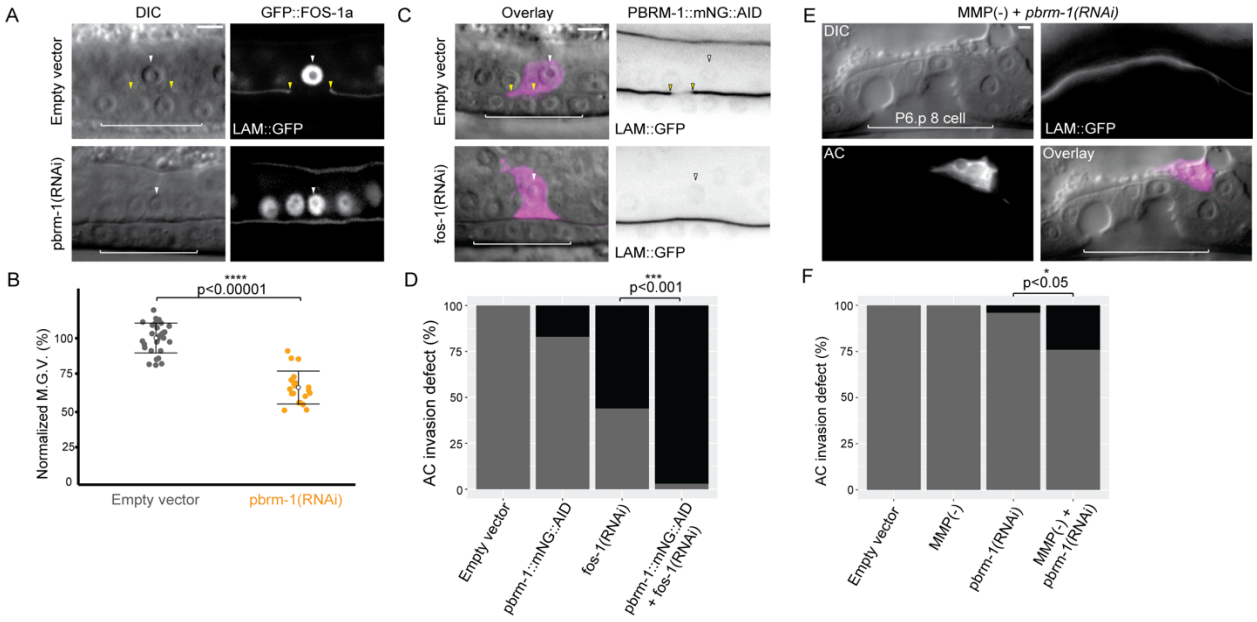

1345

1346 **Figure S8. PBAF partially regulates the FOS-1 transcription factor. (A)** Representative DIC (left) and fluorescent (right) micrographs depicting expression of endogenous GFP::FOS-1a and BM (*laminin::GFP*) in control (top) and *pbrm-1(RNAi)* treated (bottom) animals. **(B)** Quantification of GFP::FOS-1a expression in ACs of control and *pbrm-1(RNAi)* treated animals, normalized to mean expression of control group. Statistical comparisons were made between expression in the AC in control and RNAi-treated animals using Student's *t*-test (n≥20 for each condition; p value is displayed above black bracket). **(C)** DIC-Fluorescence overlay (left), and PBRM-1::mNG::AID and BM (LAM::GFP) (right), in animals treated with empty vector control (top) or *fos-1(RNAi)* (bottom). **(D)** Stacked bar chart showing percentage of AC invasion defects corresponding to each treatment and genetic background in C (n≥30 animals per condition, p values for Fisher's exact test comparing invasion defect penetrance in wild-type animals treated with *fos-1(RNAi)* and *pbrm-1::mNG::AID* animals treated with *fos-1(RNAi)* is displayed above black bracket). **(E)** Representative DIC (top-left), BM (LAM::GFP, top-right), AC (*cdh-3>PH*, bottom-left), and overlay (bottom-right) of P6.p 8 cell vulva in an MMP-deficient (-) animal treated with *pbrm-1(RNAi)*. **(F)** Stacked bar chart showing percentage of AC invasion defects corresponding to each treatment and genetic background in E (n≥30 animals per condition, p values for Fisher's exact test comparing invasion defect penetrance in wild-type animals treated with *pbrm-1(RNAi)* and MMP(-) animals treated with *pbrm-1(RNAi)* is displayed above black bracket).

1347 **SUPPLEMENTAL TABLES**

1348 **Table S1. CRFs assessed for AC invasion contribution** (see excel file)

1349 270 chromatin regulating factors targeted by RNAi for AC invasion defects. n≥30 animals
1350 for each RNAi clone. For each RNAi clone tested, the corresponding genetic sequence
1351 name, public name, protein annotation, and human homolog (HUGO Gene
1352 Nomenclature) from www.wormbase.com is given. Penetrance for each invasion defects
1353 is given as the % of animals with ACs that fail to invade the BM at the P6.p 4 cell stage
1354 out of the total number of animals assessed (Block/Invasion+Partial). Partial refers to
1355 cases where an animal had a breach in the BM narrower than the width of the basolateral
1356 surface of the invading AC. Genes in bold were recovered as significant regulators of AC
1357 invasion (Table S2). Annotations were mined from the STRING consortium www.string-
1358 db.org. Asterisks in human ortholog column denote genes with > 5 detected human
1359 orthologs, for which only the first 5 returned orthologs were listed. N.A. denotes genes for
1360 which no human ortholog exists. List is organized alphabetically based on genetic
1361 sequence name.

1362 **Table S2. Significant regulators of AC invasion** (see excel file)

1363 41 chromatin and chromatin regulating factors (CRFs) identified as significant regulators
1364 of AC invasion. For each RNAi clone listed, the corresponding genetic sequence name,
1365 public name, and human homolog is listed. AC invasion scoring data is provided for each
1366 clone at the P6.p 4 cell stage. Genes were determined to be significant AC invasion
1367 regulators if RNAi targeting resulted in ≥ 20% loss of invasion at the P6.p 4-cell stage
1368 (n≥30 animals). Genes in bold are components of the SWI/SNF complex. Asterisks
1369 denote genes previously published to regulate *C. elegans* AC invasion. N.A. denotes

1370 genes for which no human ortholog exists. List is organized alphabetically based on
1371 genetic sequence name.

1372 **Table S3. Enhanced (T444T) RNAi vectors used in this study** (see excel file)

1373 **Table S4. Strains used in this study** (see excel file)

1374 **Table S5. CRISPR reagents** (see excel file)

1375